C.P. No. 519
(22,165)
A.R.C. Technical Report

C.P. No. 519
(22,165)
A.R.C. Technical Report

MINISTRY OF AVIATION

AERONAUTICAL RESEARCH COUNCIL

CURRENT PAPERS

Wind Tunnel Measurements of the Lift-Dependent Drag of Thin Conically Cambered Slender Delta Wings at Mach Numbers 1·4 and 1·8

by

M. S. Igglesden, B.A., A.F.R.Ae.S.

LONDON: HER MAJESTY'S STATIONERY OFFICE

1960

SEVEN SHILLINGS NET

C.P. No. 519

U.D.C. No. 533.693.3 : 533.69.032 : 533.6.013.12

Technical Note No. Aero 2677

April, 1960

ROYAL AIRCRAFT ESTABLISHMENT

WIND TUNNEL MEASUREMENTS OF THE LIFT-DEPENDENT DRAG OF THIN CONICALLY CAMBERED SLENDER DELTA WINGS AT MACH NUMBERS 1.4 AND 1.8

by

M. S. Igglesden, B.A., A.F.R.Ae.S.

SUMMARY

Lift and drag have been measured, at Mach Numbers 1.4 and 1.8, on two sets of thin slender delta wings (aspect ratio 4/3) with differing degrees of conical leading edge camber, one set having drooped edges, and the other having edges shaped to give parabolic upwash distributions over the cambered part. An uncambered wing was included. All had sharp leading edges.

The absence of a realistic thickness distribution is thought to have led to unfavourable pressure fields such that separation-free flow was never achieved, and to this is attributed the failure to realise the theoretical drag reductions at the design lift conditions.

Information on the effective leading-edge suction, the nature of non-linearities in lift curve slope and the influence of free and fixed boundary layer transition on the chord force is presented and discussed.

LIST OF CONTENTS

LIST OF APPENDICES

LIST OF TABLES

LIST OF ILLUSTRATIONS

LIST OF ILLUSTRATIONS (Cont'd)

1 INTRODUCTION

The effect of conical camber in reducing the lift-dependent drag of slender wings at supersonic speeds has been the subject of recent theoretical treatments, (e.g. Ref.1). As a preliminary experimental approach, a set of thin wings has been prepared with which to investigate the effectiveness of two forms of simple camber shapes as suggested by Brebner[2]. In his paper, Brebner prescribed the downwash distribution outboard of the camber shoulder (described by the ray $\bar{\eta}$) in the form

$$\frac{w}{KV} = a + b\,(\eta - \bar{\eta})^n$$

and then deduced the required form of camber using slender-wing theory. He found that most of the available gain in lift-dependent drag should be achieved if n is no greater than 2. In this form the downwash is, of course, parabolic and the camber line is a curve whose curvature appears reasonable from the point of view of flow attachment. Appreciable gain should also be obtained from the case where n = 0. Here, the downwash steps down at the cambered part of the wing, which consists merely of a drooped leading edge.

The problem of the separated flows which occur on a sharp edged wing when the attachment line is not along the edge is avoided in this approach; it is assumed that at design C_L, when attachment is along the edge, the flow affecting the wing chord force will be like that on an uncambered wing at zero incidence. Thus at design incidence, the drag should be compounded of the zero lift drag of an uncambered wing together with the calculated lift-dependent drag using attached flow theory.

To gain some information on the closeness with which the theoretical figures could be approached, the tests were carried out on one uncambered wing, three cambered wings with leading edge droop of increasing droop angle (the least corresponding to a design lift coefficient of 0.1) and three designed according to Brebner's form n = 2, for design lift coefficients of 0.1, 0.2 and 0.3, the camber in each case lying outboard of the ray $\bar{\eta} = 0.85$. At these lifts, flow should be attached all along the leading edge and the theoretical attached flow values of lift and drag should be achieved.

The manufacture of such wings with a representation thickness distribution (for example, a Lord V, with diamond cross sections) is extremely expensive and protracted and it was thought desirable to avoid this at this stage.

The models were therefore made nominally without thickness, being of 1/16 in. mild steel plate with chamfered sharp edges. The base was left blunt. They were thus of a novel construction for supersonic testing, though the use of flat plate planforms in low speed tunnel work is by no means new.

Since all models had the same surface area and base area, differences in drag could be ascribed only to the effects of camber though the effects on skin friction of such separations as might occur, could not be distinguished. The Reynold's number was small (about 1×10^6 on root chord); transition was free in all but a few supplementary tests.

Tests were carried out during 1958 in the R.A.E. No.18 (9 in. x 9 in.) supersonic wind tunnel at Mach numbers of 1.4 and 1.8 giving values of the slenderness parameter, $\beta s/c_r$ of 0.33 and 0.5. Stagnation pressure was atmospheric in all tests. Normal force, chord force and, in a limited test, pitching moment were measured over an incidence range of about -6° to $+12^\circ$, the yaw angle being zero throughout.

2 TEST EQUIPMENT

2.1 Models

The seven models were constructed from 1/16 in. mild steel plate, (Fig.1). The uncambered model presented no difficulty. The cambered wings were a new departure in supersonic model making; they were laid out and chamfered while flat, and then dressed over on bend blocks whose external form corresponded with the required underside shape. It was found that this gave the underside shape with good accuracy with very little further work. The external shape was then finished, in the case of the drooped edges by grinding the flat surfaces, (Fig.2), while the curved cambered edges were finished by hand using a Taylor Hobson Turbine Blade Edge Projector, in which the wing profile could be compared, at 40 × magnification, with enlarged sections drawn in Indian Ink on high-stability plastic sheet, (Fig.3). This particular projector had a field of view of only $\frac{1}{4}$ in., so that the cambered part of the wing at the trailing edge could just be accommodated.

All the models had the same chord and the same developed area. This meant that the plan areas became less as the amount of camber increased, and the aspect ratio also decreased. However it was felt that this was the correct approach as it implied that one should find the best way of manipulating a given area of wing, rather than adding area to a given wing. The principal dimensions are shown in Fig.1. The developed area is 5.401 sq in. The edges were nominally of 0.001 in. radius, while the trailing edge was blunt. Although the base pressure then formed a large proportion of the total zero lift drag, this eased the model-making considerably, and seemed as likely to give consistent results as any other arbitrary trailing edge treatment.

2.2 The balance

In order to interfere with the simple design of the basic wings as little as possible, the models were fitted into a fork-end in the sting, (Fig.4). Thus the mounting "body" was identical for all wings. The sting itself carried a strain gauge bridge to measure normal force, and was mounted on a centre strip "drag" unit (which in fact measures a chord or axial force subject to a normal-force interaction due to misalignments and deflections). The sting was made as stiff as possible to reduce sting deflection; in this way the "body" could be kept as small as possible in spite of the requirement that the mouth of the fixed wind shield should be sheltered behind it over the whole range of incidence (-6 to +10.5° at Mach number 1.4). This requirement of high stiffness precluded the use of a separate pitching moment bridge whose gauge stations would have weakened the sting, but in a subsequent test, the moment at the forward normal force station was measured by a method described later. The normal force balance was designed to measure a force of 10 lb.

The centre strip axial force unit is of a type described elsewhere[3]. It was designed for a maximum force of $1\frac{1}{4}$ lb. It suffers from an inherent normal force interaction on its sensitivity, but otherwise is a satisfactory device for the measurement of small loads. It is, however, in common with other elastic mechanisms subject to vibration, and the natural frequency of the masses of the model, sting and the associated half of the drag unit carried by the flexible centre strip is about 70 c.p.s. At such a frequency there is little inherent damping and the general spectrum of vibration in tunnel shell and airstream was sufficient to cause vibration under all running conditions, with a marked resonance of high amplitude (equivalent to a fluctuating drag load of some $\frac{1}{4}$ lb on a steady drag of $\frac{1}{2}$ lb) at compressor speeds just over 4000 r.p.m. indicated, which is, of course, near 70 r.p.s. The output from the strain-gauge bridge was thus modulated at 70 c.p.s. and

this caused the automatic nulling servo device to fail. The steps taken to obviate this difficulty are described in a later section.

No similar difficulty arose in the normal force section of the balance.

Temperature effects on the specially selected groups of gauges were assumed to be limited to zero drifts. The resistance of a thermistor bead on the drag unit was used to indicate temperature there, and calibration curves of zero drifts against the "thermistor reading" were obtained which enabled corrections to be made for temperature variation.

2.3 Incidence setting

The models were mounted on the tunnel sidewall with the plane of the wings vertical. Advantage was taken of the plane surfaces facing the working section window to use a new optical method for setting model incidence to the required value under load, instead of the more usual method of setting the quadrant to the nominal angle and making a correction for sting deflection (see Fig.5).

Since a large base line (over 20 in.) is available to measure the telescope orientation, and the apparent image movement is also large, setting to within 0.05° is easy and an accuracy of 0.01° is possible with a little care (mainly in setting the telescope orientation). For zero setting, reflection off the far wall of the tunnel was used. Correction should be made for the wall's slight angle to the tunnel centreline to allow for boundary layer growth, if extreme accuracy is required, but in any case the flow direction is not exactly aligned with tunnel centreline and the wall angle can be included in the correction made for flow deviation (derived in this case from the zero lift angle for the flat, uncambered, wing).

For calibration purposes, true normal force was applied (in a horizontal direction) by weights hanging from a nylon mono-filament passing over a pulley attached to the telescope and aligned with its optical axis. By centralising the image of the light, now reflected from the calibration bar, the force was always applied at right angles to the calibration bar surface, however it might deflect.

2.4 Recording equipment

The strain-gauge bridge output was measured by the standard R.A.E. automatic equipment, consisting of a null-seeking A.C. amplifier and servo driven potentiometer in the bridge circuit. The resulting information was printed on an electric typewriter for hand computing of results.

Three features of the particular arrangements for these experiments deserve mention.

2.4.1 Thermistor bridge network

The Stantel thermistor type U 2361 was connected directly across one arm of a bridge of four 120Ω high stability resistors. Across another arm was connected a suitable resistor of about 2.7 KΩ to obtain a balance at laboratory ambient temperature of about 15° - 17°C. (Fig.6). This bridge was then connected into the standard A.C. equipment (with an input voltage of only 2 volts, as the usual voltage of 6 volts had been found to damage a thermistor bead) and readings could be obtained just as if it were a strain-gauge bridge. Sensitivity at the lowest equipment sensitivity setting was about 10 divisions per degree C (i.e. a full scale range of about 10°C). If a lower sensitivity is required, 2KΩ resistor in series with the thermistor and an additional 2KΩ in the balancing resistor (now about 4.7 KΩ) will roughly halve the sensitivity. It also

reduces the heating current in the thermistor and so allows the use of 4 volt bridge supply. Since the overall sensitivity can be recovered by increasing the equipment sensitivity, this system will in fact be used in any further applications.

A balancing capacitor is also required; a variable condenser of about 250 pF gives a suitable range to compensate for the capacity in the leads from the thermistor to its bridge circuit.

2.4.2 Filter circuit, against drag unit vibration

To enable the servo system to operate in the presence of drag unit vibration, it was found necessary to remove the modulator frequency. This was achieved by a prototype filter of the twin-T type. (Fig.7). This was arranged as a sharp cut filter to remove the bridge supply frequency (nominally 625 c/s but in practice nearer 645 c/s) and then to feed back negatively the remainder, so obtaining finally a clean 645 c/s signal.

By comparison of the filter input and output signals, on a twin beam oscilloscope, and by the use of the hand operated controls on the filter it was possible to ensure that the two signals were of approximately equal amplitude and phase. If the phase, in particular, was allowed to change through the filter, the servo units would first give an incorrect reading and then, if the quadrature increased, the balancing would become sluggish and finally completely ineffective.

2.4.3 Back-to-back servos for simultaneous normal force and pitching moment

It has already been explained that, for reasons of sting stiffness, only one pair of gauge stations was provided. J.R. Anderson suggested that it should be possible to arrange one set of servo equipment to measure the normal force bridge complete, and another set simultaneously to measure a bridge consisting of one pair of the normal force gauges and a second pair of "dummy" gauges kept in an unstrained condition; the latter bridge would measure the bending moment and hence the pitching moment at that gauge station. (Fig.8). Since the servo system is a nulling system, if each side were balanced, there should be no interaction. As a supplementary experiment, this arrangement was tried and worked well. There is no sign of any instability in the present conditions.

2.5 Oil flow technique

At the small scale of these models, the commonly used mixture of Titanium Oxide and oil was not found to be satisfactory. Since the models were of untreated steel, a dark-coloured material was sought, and after several tests a mixture of engineer's marking blue (prussian blue in oil) with oleic acid was used successfully. (See Appendix 1 for details).

3 REDUCTION AND PRESENTATION OF DATA

3.1 Calibration

Details of the calibration technique, using true normal and axial loadings, are given in Appendix 2.

3.2 Reduction of results

Lift and drag can be obtained from normal-force and chord-force by the usual means, which requires that the angle between the stream and the model surface axes shall be known. As previously mentioned, it has been assumed that the uncambered model is truly plane (and this indeed was confirmed by

testing the model inverted) and therefore that its setting at zero lift gives the flow deviation; thus the difference between the particular wing setting and the zero-lift setting for the uncambered wing gives the incidence of the wing.

The normal-force and chord-force referred to zero-lift axes are also required for analysis of lift-dependent drag. This change of axis is carried out using the angle between the wing surface and the zero-lift angle of the wing; this is the difference between the zero-lift setting of the wing and the zero-lift setting of the uncambered wing.

It should be noted that these final results can only be calculated when the zero-lift angles have been obtained by plotting lift (or normal force) against setting angle. Therefore the normal-force and chord-force referred to wing-surface axes were first computed.

In reduction of the data to coefficient form, it has been thought preferable to use the developed area of the wings, which is the same for all models in the series. Any improvements then show what is to be gained by alteration of shape of the basic wing. If plan area is used as the basis, then the cambered wings are, in effect, bigger wings and it may not be clear if improvements are due to this additional area (for example, compare the effect of end-plates, which do not increase wing plan area).

However, if the results presented here are used individually and out of context, it should be borne in mind that drag coefficients and lift coefficients should be increased and lift-dependent drag factors decreased by the ratio of developed to plan area. (Table 1).

3.3 Results

Drag polars (C_D v. C_L) and lift curves (C_L v. α) are shown in Figs.9-12. These are the direct results from the measured chord-force and normal-force, transition free, and exhibit marked "laminar buckets" in the drag polars of the uncambered model, A, at both the test Mach numbers 1.4 and 1.8.

The lift curves are plotted against incidence based on the zero-lift angle as datum. The incidence corresponding to the flat part of the wing lying along the stream is indicated for each wing.

In Figs.13-18 are shown chord-force against normal-force. Here the axes again refer to zero-lift. For models A and E, (Figs.13-16) the incremental chord-force with transition fixed by wires is shown, and the deduced chord-force obtained by correcting for the laminar effects.

4 DISCUSSION

4.1 Lift curves

The curves do not show those non-linear characteristics which would be expected for sharp-edged slender wings. For the most heavily cambered wings, the results are linear over the whole range from about -6° to $+10^\circ$ (C_L -0.2 to +0.3). For the uncambered wing and the less cambered wings, the lift is linear over a range of several degrees incidence near zero, but outside this range, a kink occurs beyond which the slope is greater, though once more linear.

These characteristics appear at both Mach numbers, and have been verified by carrying out the tests at unusually small increments of incidence (viz. one eighth degree intervals).

For all wings, over the incidence range tested, the slope is less than slender wing theory predicts, but is fairly close to the linear theory result. Thus, the heavily cambered wings have a slope near linear theory at each Mach number, but the less cambered wings, and particularly the uncambered wing, have a slope which is less than linear theory suggests in the low incidence range and greater outside the kinks. Thus at an incidence of about 8° (C_L 0.25) all but the uncambered wing have a lift close to the linear theory, based upon their developed areas.

Considered individually, on plan area, the inner region slope for all the cambered wings is near the linear theory result (that for the uncambered wing being some 10% less which may be accounted for by viscous effects on the circulation) while in the outer regions, the slopes are similar for all wings except the most heavily cambered of each set, the slope being some 10% higher than the linear theory prediction.

It has been suggested that the kinks are an effect of the ridges formed by the chamfers; a test on a wing with the same thickness but with chamfer on one side only showed kinks bounding a region of the same width (-1° to $+3\frac{1}{2}^{\circ}$ compared with $-2\frac{1}{4}^{\circ}$ to $+2\frac{1}{4}^{\circ}$), but when the chamfered side was built up to a central ridge over about two thirds of its length, thus removing the chamfer ridges, kinks still appeared, the outer sections still having similar slopes but the inner region having its slope even further reduced (Fig.19). It therefore seems that the presence of ridges does not cause this phenomenon.

It is, in fact, much more likely that it is associated with the presence of vortices. For the uncambered wing, the kinks correspond with the occurrence of well developed separations, but the correlation is less well established for the cambered wings. (See Section 4.5).

4.2 Centre of pressure

Centre of pressure positions were measured for models A and E at both Mach numbers 1.4 and 1.8. In each case, the position of the centre of pressure was found to lie at 0.66 root chord from the apex, within an experimental accuracy of about 2% root chord at lift coefficients above 0.1. At lower lift coefficients the accuracy rapidly deteriorates due to the low values of both lift and pitching moment.

There was thus no detectable effect of conical camber on the centre of pressure position.

4.3 Drag

In this discussion of the drag results, the emphasis will be mainly on the uncambered wing (A) and the cambered wing of least surface curvature (E, designed for parabolic downwash, design lift coefficient 0.1). The latter has always been considered the most likely to achieve fully attached flow: although that promise has not been realised, the results, as will be shown, are nevertheless quite encouraging.

4.3.1 Zero lift drag

For the purpose of the experiment, the absolute value of the zero lift drag of each wing is of no interest, but the difference between the drag at lift of the cambered wings and the zero lift drag of the uncambered wing is the important feature under investigation. It is therefore essential that those components of drag not dependent on lift should be identical for all wings. An estimate of the wave drag, skin friction and base drag shows them to be roughly equal in magnitude (Table 2). Measurement of base drag was not attempted in view of the small size of the models, while transition was left

free because it was considered difficult to ensure that transition fixing devices were exactly identical for each model and also because any excrescences would markedly alter the geometric profile of these thin wings. It was therefore hoped that, if similarity of flow (i.e. full attachment) was achieved between the uncambered model at zero lift and the cambered models at some incidence, near their design conditions, these two items (base drag and skin friction) would also be similar; if the theoretical results were obtained, it could then be assumed that similarity in these respects had been achieved.

4.3.2 Skin friction effects

When the results for wing A were plotted, (Figs.13 and 15) a reduction in chord-force at small lifts was at once obvious, in the form of a "bucket" and this effect was ascribed to a large area of laminar flow at these small incidences (less than $1\frac{1}{2}^{o}$). This was substantiated by boundary layer investigation using sublimation techniques. Chord-force was roughly constant with incidence except in this region, and it was therefore assumed that this constant value could be used as the value for "transition fixed" zero-lift drag.

The chord-force for the cambered wings showed no such marked skin friction effect, but the general form of the chord-force was different and might have obscured the effect. Examination of the boundary layer by sublimation of ace-naphthalene was inconclusive since the resulting patterns were obscured by the similar sublimation effects due to flow separations.

As a subsidiary experiment, boundary layer trip wires were attached to the chamfered faces of wings A and E. These were 0.005 in. wires stuck on with 0.0025 in. thick Sellotape of about 0.15 in. width. The wires were placed about half way up the faces (about 0.125 in. from the edges and parallel with them) where the local wing thickness was about 0.030 in., only four times the height of each trip.

The lifts and pitching moments were not affected by this, but the chord-force of model A now showed no "laminar bucket". The total chord-force increment due to the trips was constant with normal-force except in the "laminar bucket" region, where it bulged steeply (Figs.13 and 15). It was decided to use this bulge as the correction to "transition free" results to obtain a "transition fixed" value without the wire wave drag.

A similar result was found with model E. The laminar effect was not as great as with the uncambered wing, but was quite obvious when the chord-force increment was examined (Figs.14 and 16). There was some difference between the values of the constant increment outside this region at positive and at negative incidence, due possibly to different degrees of shielding of the wires in the separated flow from the edge. The rise in increment above a mean value was taken for correction of the "transition free" results.

4.4 Lift-dependent drag factors

The lift-dependent drag depends upon the lift-curve slope and the chord-force variation with lift. If chord-force does not vary with lift, the lift-dependent drag is the normal force component in the drag direction, and the lift-dependent drag factor ($K = \pi A\, C_{D_i}/C_L^2$) in slender wing theory is 2. In linear theory it is somewhat greater than 2 to the extent that the lift-curve slope is less than $\pi A/2$.

The leading edge suction, which is possible with subsonic leading edges, gives a reduction in chord-force with lift. This, in slender wing theory, amounts to half the normal-force component, and the lift-dependent drag factor is then reduced to 1. In linear theory, it is greater than 1.

It is convenient to use as a datum, the R.T. Jones "minimum bound for not-so-slender wings" (which includes the lift-dependent wave drag) which gives the lift dependent drag factor:

$$K_{R.T.\ Jones} = 1 + 2\left(\frac{\beta s}{C_o}\right)^2$$

In the present experiment, we have lift-curve slopes near to the linear theory figures and we should therefore hope to achieve a reduction in chord-force with lift similar to the theoretical leading edge suction term in linear theory, if we are to obtain lift-dependent drag factors near those predicted by Brebner.

Thus discussion of the results will be focussed on the chord-force results which are a powerful indication of the degree to which the lift-dependent drag of the cambered wings has been reduced below that of the uncambered wing.

The models are now considered in turn.

4.4.1 Model A

The sharp-edged uncambered wing A shows an almost negligible degree of effective leading edge suction, while at low lift coefficients, the lift curve slope is no greater than linear theory predicts. Thus the lift-dependent drag factor

$$K = \frac{C_D - C_{D_o}}{C_L^2}\ \pi A$$

is near the linear theory value for the particular value of the slenderness parameter $\beta\ s/C_o$ with the suction term omitted.

At lift coefficients above 0.1, the lift exceeds the linear theory predictions and the lift-dependent drag factor falls to a value slightly less than the linear theory value (Fig.20).

4.4.2 Model E

The induced drag factor for individual wings in the family of cambered wings is defined as

$$K = \frac{C_D - C_{D_{o_{uncambered}}}}{C_L^2}\ \pi\, A_{uncambered}$$

where the coefficients are based on the developed areas of the wings (which are all equal).

Since it is hoped that the non-lift-dependent drag of the cambered wings at their design C_L, when flow should be fully attached, would be the same as that of an uncambered wing when its flow is fully attached (i.e. at zero lift) the theoretical value of K for the cambered wing at design lift should be near the theoretical value of the uncambered wing allowing for the leading edge suction term. As Brebner[2] has demonstrated, for the conical camber shapes he discusses, and with the camber outboard of 85% semi-span, the slender wing values are 1.17 and 1.08 compared with 1.00 for a flat wing with attached flow, (or for Smith's "wavy" cambers of high enough exponent[1])

and 2.00 for a flat wing with the suction term omitted. For not-so-slender wings, the target value of K is appropriately a little higher than the linear theory values including the suction term.

As may be seen in Fig.21, this target is not achieved although the values of K actually found at the design lift coefficient are better than those for the flat wing at the same lift coefficient and $\beta s/C_o$.

This failure is largely due to the fact that, at design incidence the flow is not fully attached. As can be clearly seen in the oil flow photographs, (Fig.22) there are separations from both upper and lower surfaces. This follows from the fact that the theoretical pressure distribution in cross-flow planes near the edge of a thin wing with conical camber of this type has pressure peaks, negative on the upper surface and positive on the lower, (Fig.23). Furthermore, the curvature of the streamlines on the upper surface is in the unfavourable sense (the pressure rises inwards). Unfavourable pressure fields therefore exist inboard of the upper surface peak, near the chamfer shoulder, and outboard of the lower surface peak, very near the edge. The effect of separations will be to modify the theoretical pressures, giving increased drag.

Because of these separations, it is impossible to discover if the design method is effective in producing attached flow at the leading edges at the required incidence.

There is, however, a reduction in chord-force with incidence as shown in Fig.24 where chord-forces for the uncambered wing and for wing E are compared. Taking the "transition fixed" values it can be seen that the chord-force of wing E is less than that of wing A above a normal force coefficient of about 0.08 at $M = 1.4$ and rather less at $M = 1.8$. The observed reduction of chord-force with positive normal force, levelling off markedly at a certain value of the normal force, is qualitatively similar to the behaviour of the leading edge suction force on a rounded edge, which increases with normal force until it is limited by the pressure dropping to near vacuum conditions at the point of lowest pressure on the leading edge. At $M = 1.4$, the maximum reduction of chord-force coefficient of wing E is 0.006; this, and the similar reduction at $M = 1.8$, is about twice the value predicted for an uncambered wing of the present thickness according to the factors suggested by Cane and Collingbourne. (The predicted value is not actually achieved on wing A, because it undergoes edge separation at a normal force coefficient of about 0.03). The behaviour of the cambered wing may be due to the greater effective leading edge thickness and frontal area of the down turned edges, in which case the more heavily cambered wings might be expected to show even greater reductions in chord-force. In fact, this does happen, and it is only wing B at $M = 1.4$ that shows the limiting condition within the experimental range of normal force.

In appears from these results that, had the separations at design incidence been absent, (perhaps by the use of a suitable thickness distribution, to avoid unfavourable pressure fields) the cambered wings might well have produced the theoretically predicted low lift-dependent drag.

This strongly emphasises the necessity for avoiding, in experiments, separations of a type which will not occur on practical wing shapes, and this implies that usually the correct thickness distribution will be essential in models. However, it must be pointed out that, at present, it is not known what degree of adverse pressure gradient, streamwise and spanwise, can be admitted, so that it is not possible to specify in advance what minimum thickness distribution is required. The effect of Reynold's number on these phenomena has also to be taken into account when unfavourable fields exist.

4.4.3 A general description of the lift-dependent drag of thin cambered wings

It has been observed that the measured drags of all the cambered wings tested, although they do not achieve the low lift dependent drag relative to the uncambered wing which was hoped for, because of the extensive separations at all incidences, do nevertheless show a reduction in chord-force with incidence such that they have low values of lift-dependent drag relative to their own zero lift drags.

A difficulty which must be resolved at once is that, as has already been stated, the tests were carried out with transition free. In the two cases where transition was fixed, the differences in drag caused by the transition wires indicated that the "transition-free" chord-forces of these wings incorporated a "laminar bucket". The application of the correction for this to the transition free values for model E resulted in a chord-force to normal force relationship which indicates some sort of consistent behaviour, in contrast with the "transition-free" measurements.

Examination of the similar results for the other cambered wings showed that the addition of a similar correction to these would cause them to fall into a similar pattern, and failing any other information, the correction obtained for model E was applied to all the other cambered model results (Figs.17 and 18). It can be seen that, except for model G, the resulting relationship between chord-force and normal-force is again well behaved, while model G needs a rather larger correction to bring it into line.

The chord-force to normal-force relationship is then seen to be as follows:-

(1) at negative lift, the chord-force is constant,

(2) from zero lift to some positive lift, chord-force drops, at a slope of roughly 0.035 (corresponding to a forward inclination of the force vector of about 2°),

(3) from some positive lift, chord-force is again constant. The point at which the limiting value is reached depends on the amount of camber.

In Fig.25, the results for all the wings are superposed, in the form $-(C_x - C_{x_o})$ against normal force $-C_z$. The linear theory suction term $\frac{C_L^2}{\pi A}\sqrt{1 - \left(\beta \frac{s}{C_o}\right)^2}$ is also shown, and it can be seen that the trend is clearly towards this value.

In view of the non-linear character of the lift curves, it may be preferable to analyse the results on the basis of αC_L. In this case, if C_D is plotted against αC_L, the slope of the resulting line is an indication of the forward inclination of the force vector. A slope at the origin of unity indicates no effective leading edge suction, while the full linear theory leading edge suction terms would give a slope which increases from 0.5 for a slender wing to 1 for sonic edges, and is 0.57 at $M = 1.4$ and 0.64 at $M = 1.8$. A constant value of the slope indicates an effective suction force proportional to αC_L (or α^2 or C_L^2 nearly) in contrast to a constant slope in the graph $-C_x$ v. $-C_z$, which indicates an effective suction force proportional to $-C_z$ (or α or C_L nearly).

For model A, the slope is unity throughout the incidence range, (Fig.26) in agreement with the almost constant measured chord-force.

For model E, the slope is near 0.5 near the origin, corresponding to nearly full leading edge suction, and is unity beyond $\alpha C_L = 0.02$ (C_L about 0.2). Other cambered wings show a slope between 0.5 and 0.7 near the origin and a slope between 0.8 and 0.87 in the range of lift coefficients between 0.2 and 0.3 (the maximum lift coefficient achieved in the tests). This suggests that nearly the full theoretical leading edge suction was being achieved at low incidence (below $C_L = 0.1$), dropping to a fairly steady value of about 25% suction beyond a lift coefficient of 0.2.

The differences already demonstrated between the lift-dependent drags of the different wings show that the drag polars cannot be described in the way postulated, for example, by Cane and Collingbourne, that is, the polars being similar but displaced so as to place their minimum drag points on a parabolic curve. In the present tests, the polars are not similar in shape; nor are the minimum drag points found to lie on a well defined curve.

4.4.4 The effect of Mach number on chord-force

The chord-force being compounded of wave drag, skin friction, base drag and effective leading edge suction, no simple similarity law could be expected to apply.

However, it has been found that empirical collapse of the results at $M = 1.4$ and $M = 1.8$ can be achieved if the factor obtained from the zero-lift chord-forces of the uncambered wing at the two Mach numbers is applied. Although the estimate of zero-lift drag of Table 2 is only rough, the ratio of drags here is almost the same.

The closeness of fit of the factored $M = 1.4$ results on the actual $M = 1.8$ results is remarkable, (Fig.27). Model D shows a nearly constant difference (the reasons for this is not known) but otherwise the correlation is very good, and this suggests that the use of Model E's "laminar bucket" correction on other cambered wings is justified.

4.5 The relation between surface flows and aerodynamic forces

The aerodynamic forces show certain characteristics which suggest that marked changes in flow may be taking place at corresponding incidences. Thus the lift curve slopes have kinks at both negative and positive incidences, while the chord force also shows "non linear" features.

On these small models, good oil flow patterns are not always easy to obtain, while the exact definition of attachment lines and other characteristics is often difficult.

Similarly, the vapour screen method has not proved particularly rewarding and no photographs worthy of reproduction have been obtained.

However the general pattern of oil flow and vapour screen together indicates the following features of the flow at Mach number 1.8.

The uncambered wing exhibited leading edge vortex separations on the upper surface at an incidence of 2°. They may have occurred at lower incidences, but they could not be detected, for example, at 1° (Fig.28). As incidence increased, the vortices grew steadily, and at the incidence of 12°, the whole upper surface was washed by the typical cross flow pattern of vortex separation with secondary and other separations of conical form.

The cambered wings showed separations (again all conical except where specified otherwise) below the cambered part, springing from the edge, at all negative incidences and at positive incidences up to about 4° above design incidence for each wing. At positive incidences, from very near zero (i.e. the uncambered surface lying in the free stream direction), a separation occurred on the upper surface, springing from near the camber shoulder (that is, the ray $\bar{\eta} = 0.85$).

At small incidence, this separation did not seem to be quite conical when judged from the oil patterns, but vapour screen showed that they were of conical form, and were certainly not closed bubbles. By design incidence of each wing, however, the surface pattern corresponded clearly to large-scale conical separations (Fig.22). Since the separation on the upper surface occurs inboard of the camber and it influences a surface which is inclined at only a small angle to the chord force direction, the reduction in chord-force will be less than that due to separation from the under surface, which occurs at the edge. It therefore appears that the lower surface separations are the more deleterious.

It was to be expected that, soon after design incidence, the upper surface separation would spring from the edge and not from the camber shoulder. This behaviour has only been detected on model B, the flow appearing to be attached on the drooped edge at 6° but not at 8° (the design incidence for this wing being about $3\frac{1}{2}^{\circ}$), Fig.29.

To connect the separation behaviour with the features of the force measurements, the diagram shown in Fig.30 has been constructed, based on the lift curves of the various wings. Regions where upper and lower surface vortices exist are shown by hatching, while the "kinks" in the lift and chord-force curves are marked.

It is concluded from this diagram that

(1) there is no obvious connection between the kinks in the lift curves and the surface flow patterns for cambered wings, but for the uncambered wing, the kinks occur close to the points where edge separations become obvious;

(2) the regions where separations occur on both surfaces simultaneously appear to straddle the design incidences of the wings (with the exception of wing G), and the portion of the chord-force curve where effective leading edge suction occurs also corresponds with this region.

5 CONCLUSIONS

(1) It has not been demonstrated that simple forms of conical camber can reduce the lift-dependent drag of a thin slender delta wing to the values associated with fully attached flow.

(2) This failure is due to adverse pressure gradients existing on both upper and lower surfaces of a cambered wing without a suitable thickness distribution.

(3) Nevertheless, at sufficiently high lift coefficient (always less than 0.3) every cambered wing has had less drag than the uncambered wing, and model E, designed for a parabolic downwash distribution at a lift coefficient of 0.1, has less drag than the uncambered wing at lift coefficients above 0.08.

This results from the fact that all the cambered wings show a degree of effective leading edge suction, which suggests that, if the unwanted separations could be suppressed (by suitably thickening the wings) notable reductions in lift dependent drag might result.

(4) The lift curve slope of the wings is generally close to that predicted by linear theory (and is thereby lower than the slender wing theory prediction) but it is marked by kinks which bound linear regions, that near zero lift having a slope less than linear theory and those outside the kinks having a slope some 10% higher than the former. The reason for the kinks is not clear but from the evidence of oil flow patterns on the uncambered wing (but not the others), it may be connected with the appearance of edge separations.

(5) The centres of pressure of both the uncambered wing and the least cambered wing were measured and found to lie close to the theoretical position at 2/3 root chord from the apex.

(6) With transition free, at the test Reynold's number of 0.35×10^6 per in., marked "laminar buckets" were detected on both the uncambered wing, and, to a slightly less extent, the least cambered wing.

(7) The uncambered, sharp-edged wing showed very little sign of effective leading edge suction.

ACKNOWLEDGEMENTS

Acknowledgement is due to Mrs. D.L. Brookman, who assisted in the tests and computed the results.

LIST OF SYMBOLS

a, b	downwash equation constants (Section 1)
a,b,c,d,e	calibration constants for strain-gauge balance (Appendix 2)
c_c	root chord
A	aspect ratio
C_D	drag coefficient*
C_{D_o}	zero lift drag coefficient*
C_L	lift coefficient*
C_p	pressure coefficient
$-C_x$	chord force coefficient*
$-C_z$	normal force coefficient*
K	co-tangent of angle of sweep (Section 1)
k	lift dependent drag factor, $\left(C_D - C_{D_o}\right)\pi A/C_L^2$
M	Mach number
n	parameter in downwash equation (Section 1)

*All force coefficients in this Note are based on the developed area of the wings (see Section 3.2).

LIST OF SYMBOLS (Cont'd)

ΔR_x ΔR_z	incremental readings from strain-gauge balance equipment
s	wing semi-span
S	wing area
V	free stream velocity (Section 1)
w	perturbation velocity in z-direction (Section 1)
X,Z	forces in x-direction (forward) and z-direction (downward) referred to wing axes
X_c,Z_c	forces referred to calibration axes
α	angle of incidence
β	$\sqrt{M^2 - 1}$
η	conical ray defined by y/x
ζ_c	angle of misalignment between wing surface and calibration bar surface

---

LIST OF REFERENCES

Ref. No.	Author	Title, etc.
1	Smith, J.H.B. Mangler, K.W.	The use of conical camber to produce flow attachment at the leading edge of a delta wing and to minimize lift-dependent drag at sonic and supersonic speeds. A.R.C. 19,961, September, 1957.
2	Brebner, G.G.	Some simple conical camber shapes to produce low lift-dependent drag on a slender delta wing. C.P.428, September, 1957.
3	Anderson, J.R.	Strain-gauge balances for wind tunnels*. A.R.C. 18,655, January, 1956.

ATTACHED

Appendices 1 and 2
Tables 1 and 2

---

*An outline of practice in the United Kingdom.

APPENDIX 1

THE USE OF "ENGINEER'S BLUE" FOR OIL FLOW TESTS

Engineer's Blue, consisting of Prussian Blue dye in oil, was obtained in ounce tins. One quarter of a tin was dissolved in about 200 c.c. of trichlorethylene, with eight drops of oleic acid. This was allowed to stand for about 20 minutes, while the larger particles of dye precipitated, and the fluid was then decanted. It was sprayed onto the model to give a thin but even glossy finish.

At the test Mach number of 1.8, it was found that the oil hardly moved until the stagnation pressure (reduced to a low value for starting the tunnel) had risen to within about 5 in. Hg of atmospheric. Although no other Mach number was used, it is thought that the oleic acid content could be adjusted to give similar results*

In use, the oil flows over the surface and most of it runs off the trailing edge, leaving fine filaments of oil in a pattern which is well developed after 5-10 minutes running.

After each run, the model was photographed and then cleaned by agitation in a small tank of trichlorethylene. After being allowed to dry, it was wiped lightly with a soft cloth. This method avoided damage to the delicate apex of the model. It was then ready to be resprayed.

---

*In other recent tests, the same mixture has been used successfully at M = 1.4 on similar models.

APPENDIX 2

CALIBRATION OF THE BALANCE USING TRUE NORMAL AND AXIAL LOADINGS

Calibration of the normal-force and chord-force strain-gauge bridges had to be performed with particular care, in spite of there being only two components (latterly pitching moment was also measured; see Section 2.7). This is because the deflection of the sting under a normal-force causes a component of this force to affect the chord-force unit whose axis is fixed in the original undeflected direction. There is therefore an interaction related to (normal-force)^2. Further, the sensitivity of the chord-force unit depends on normal-force. Thus it is necessary to cover a full range of both normal-force and chord-force to obtain sufficient data to obtain the calibration equations.

Fortunately there is no detectable interaction of chord-force on normal-force reading, while the effect of position of application of load was negligible for the expected range of centre of pressure of this set of models.

The calibration equations are then of the form

$$-Z_c = a\,\Delta R_z$$

$$-X_c = \frac{\Delta R_x + b\,\Delta R_z + c\,\Delta R_z^2}{d + e\,\Delta R_z}$$

where a, b, c, d, e are calibration constants

and $-Z_c$ and $-X_c$ are referred to axes normal to and along the calibration bar's reflecting surface.

To obtain forces referred to wing surface axes, it is necessary to correct for the angle between these axes and the calibration bar axes. This angle (ζ_c) can be measured in the laboratory with the incidence-telescope device by attaching in turn the calibration bar and the various wings to the rigidly fixed model mounting.

The angles being small (less than 0.25°) we can put

$$Z = Z_c$$

$$X = X_c - Z_c\,\zeta_c$$

The calibration equations now become

$$-Z = a\,\Delta R_z$$

$$-X = \frac{\Delta R_x + (b - ad\,\zeta_c)\,\Delta R_z + (c - ae\,\zeta_c)\,\Delta R_z^2}{d + e\,\Delta R_z}$$

where a, b, c, d, e are again constants of calibration,

and ζ_c relates to the particular model.

It may be noted that the effect of this correction for ζ_c on the ΔR_z term is of the same order as the original constant, while the effect on the ΔR_z^2 term is less than 1 percent in the present arrangement.

TABLE 1

Ratio of plan area to developed area of cambered wings

Wing	Plan Area / Developed Area
A	1.000
B	0.972
C	0.958
D	0.928
E	0.989
F	0.968
G	0.942

TABLE 2

Estimate of zero lift drag of uncambered wing

		M = 1.4	M = 1.8
Wave drag coefficient		0.004	0.004
Base pressure		0.006	0.003
Skin friction	(Laminar	0.0015	0.0016
	(Turbulent	0.0049	0.0050
Total drag	(Laminar	0.012	0.009
	(Turbulent	0.015	0.012

WT.2078.C.P.519.K3 - Printed in England

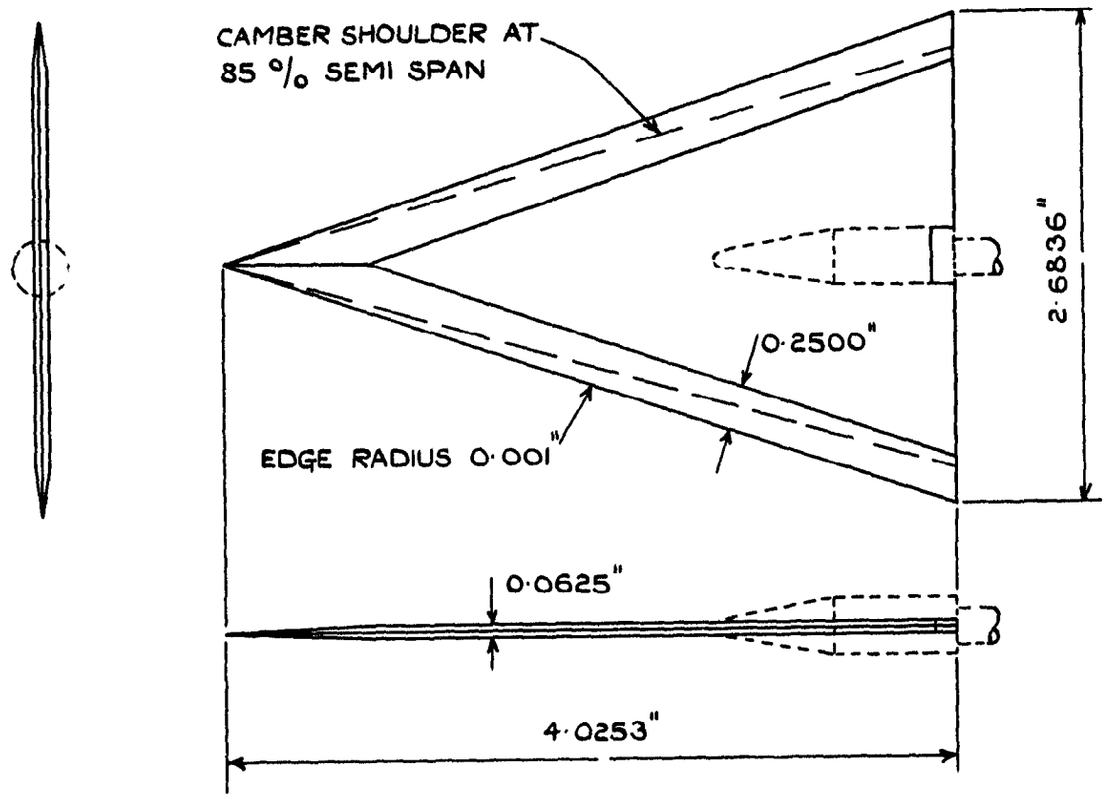

FIG. 1. BASIC WING PLANFORM AND THICKNESS DISTRIBUTION - WING A.
(OTHER WINGS DIFFER OUTBOARD OF CAMBER SHOULDERS)

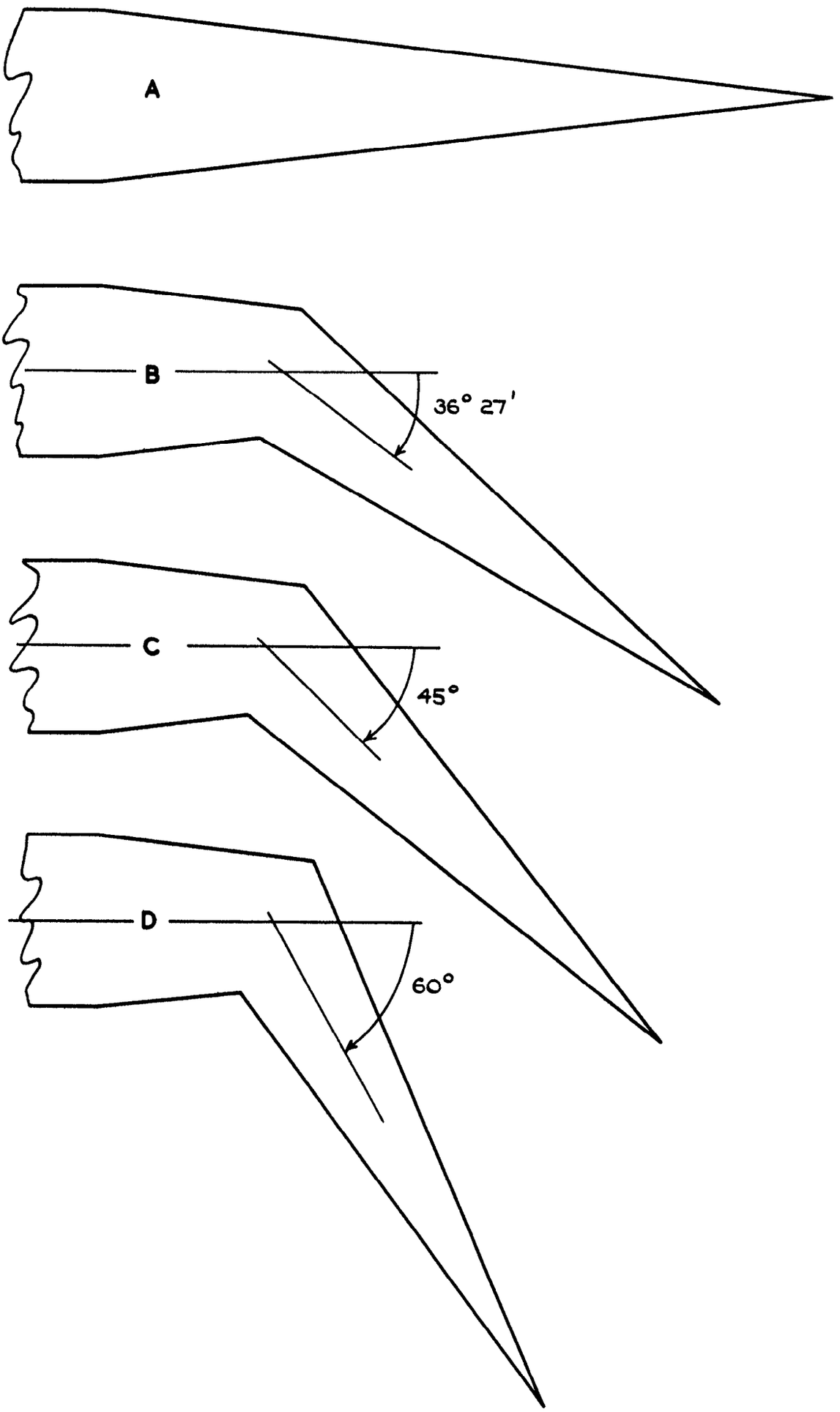

FIG. 2. WING TIP SECTIONS (ON TRAILING EDGE) OF WINGS A, B, C, D.

20 X FULL SIZE

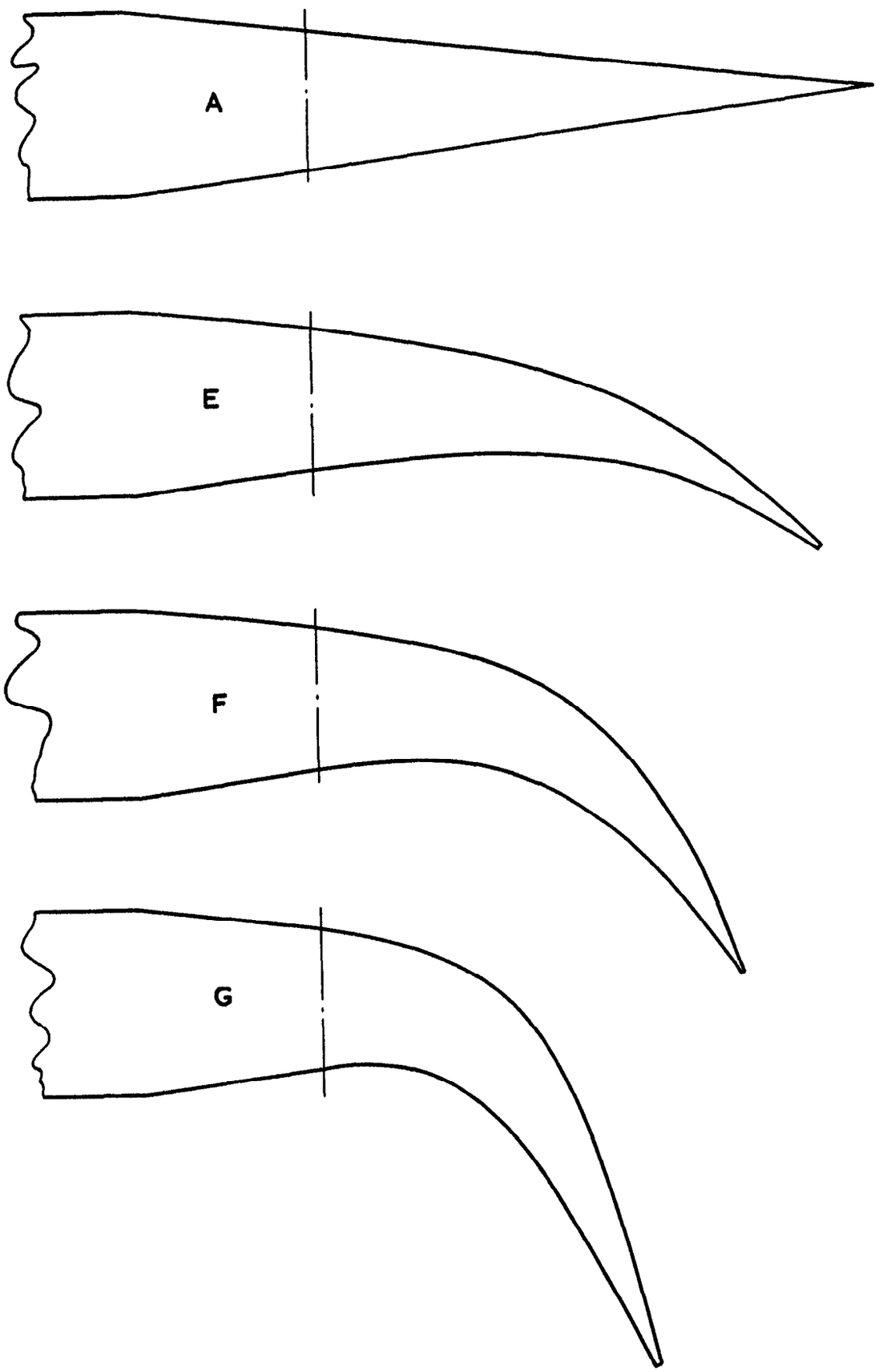

FIG. 3. WING TIP SECTIONS (NORMAL TO EDGE) OF WINGS A, E, F, G.
20 X FULL SIZE

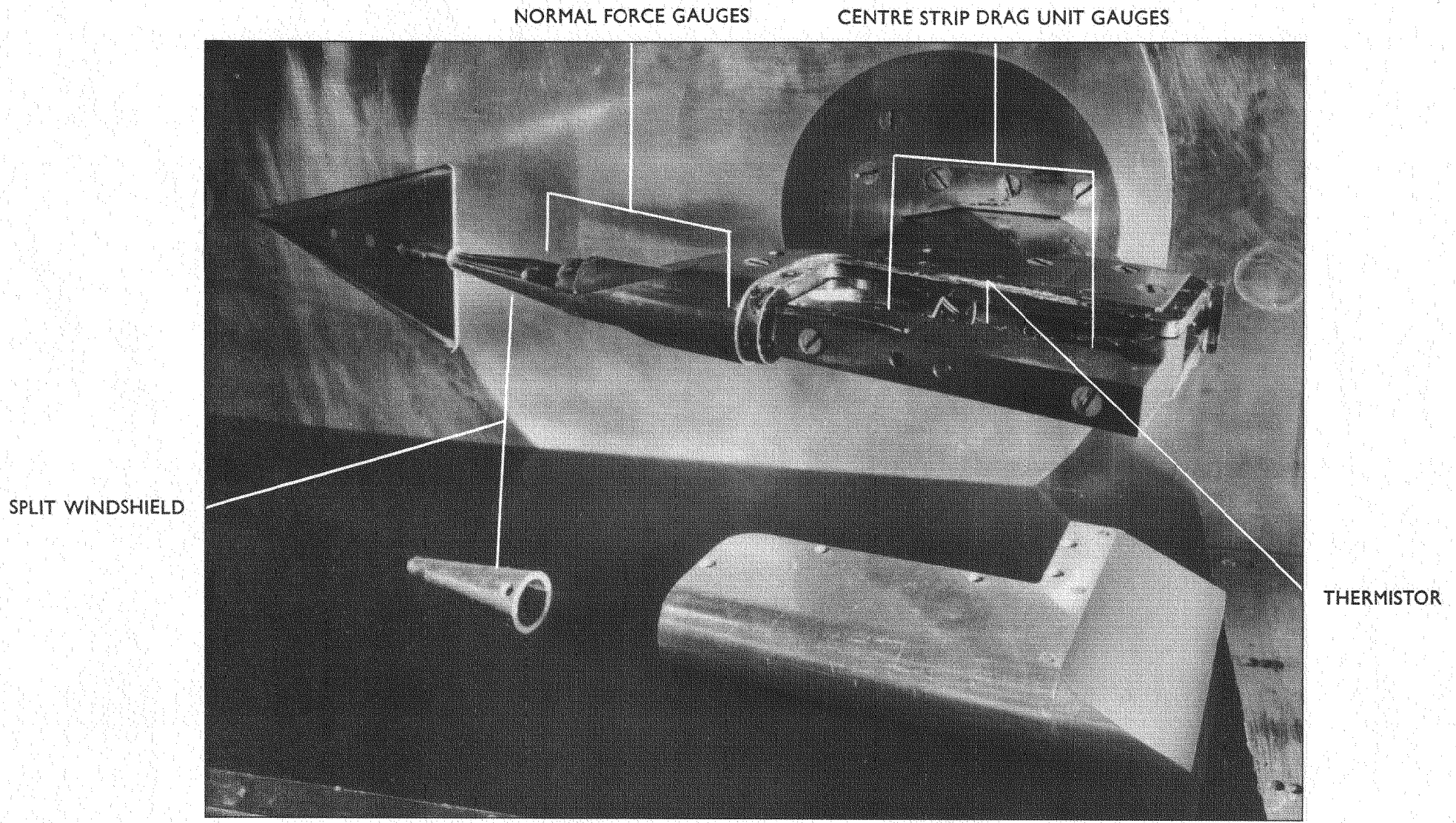

FIG.4. ARRANGEMENT OF THIN WING ON REAR STING BALANCE IN SIDE WALL MOUNTING IN R.A.E. No.18 (9″ x 9″) WIND TUNNEL

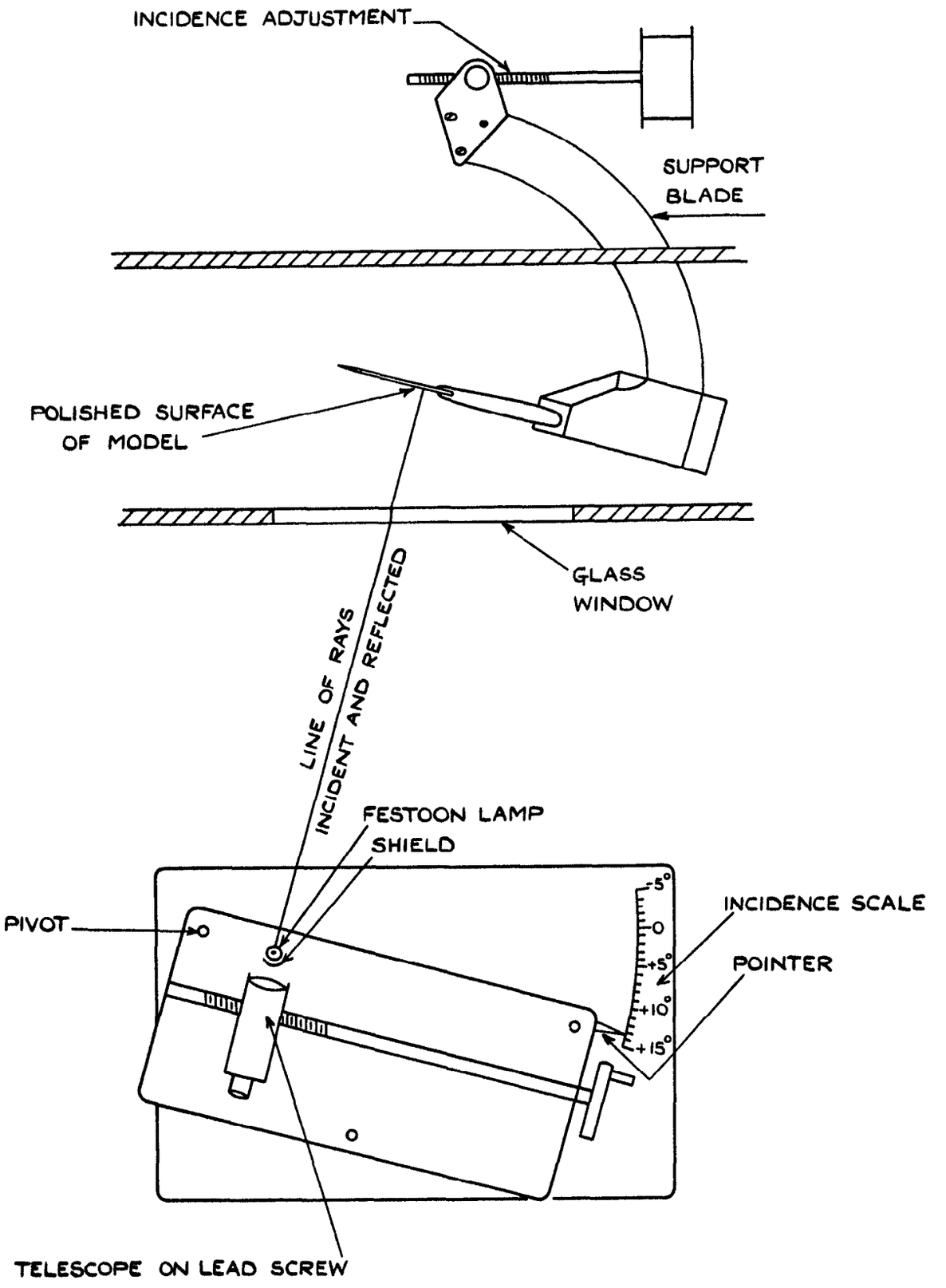

FIG. 5. ARRANGEMENT OF INCIDENCE SETTING SYSTEM.

(NOT TO SCALE)

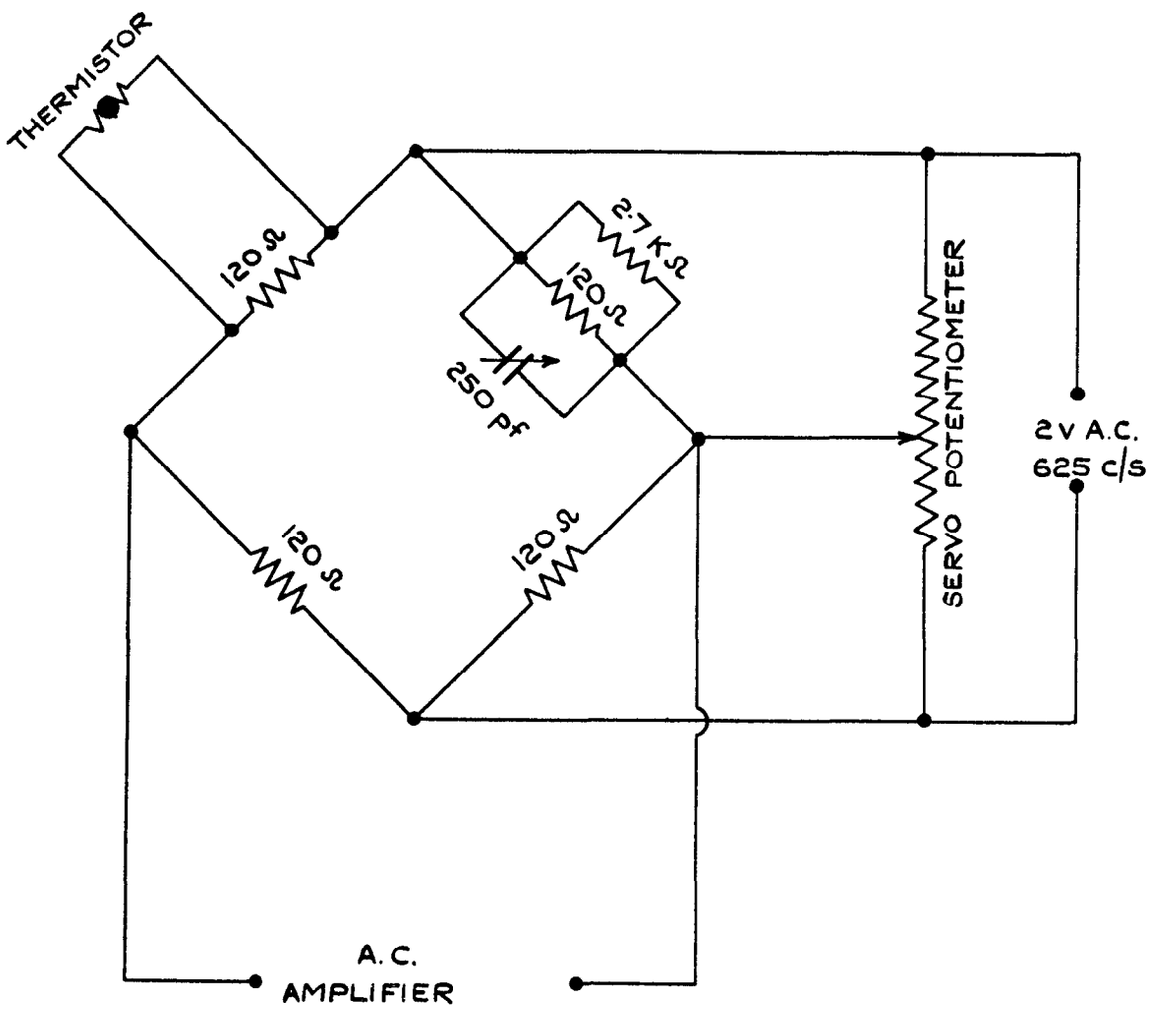

FIG. 6. ARRANGEMENT OF THERMISTOR BRIDGE.

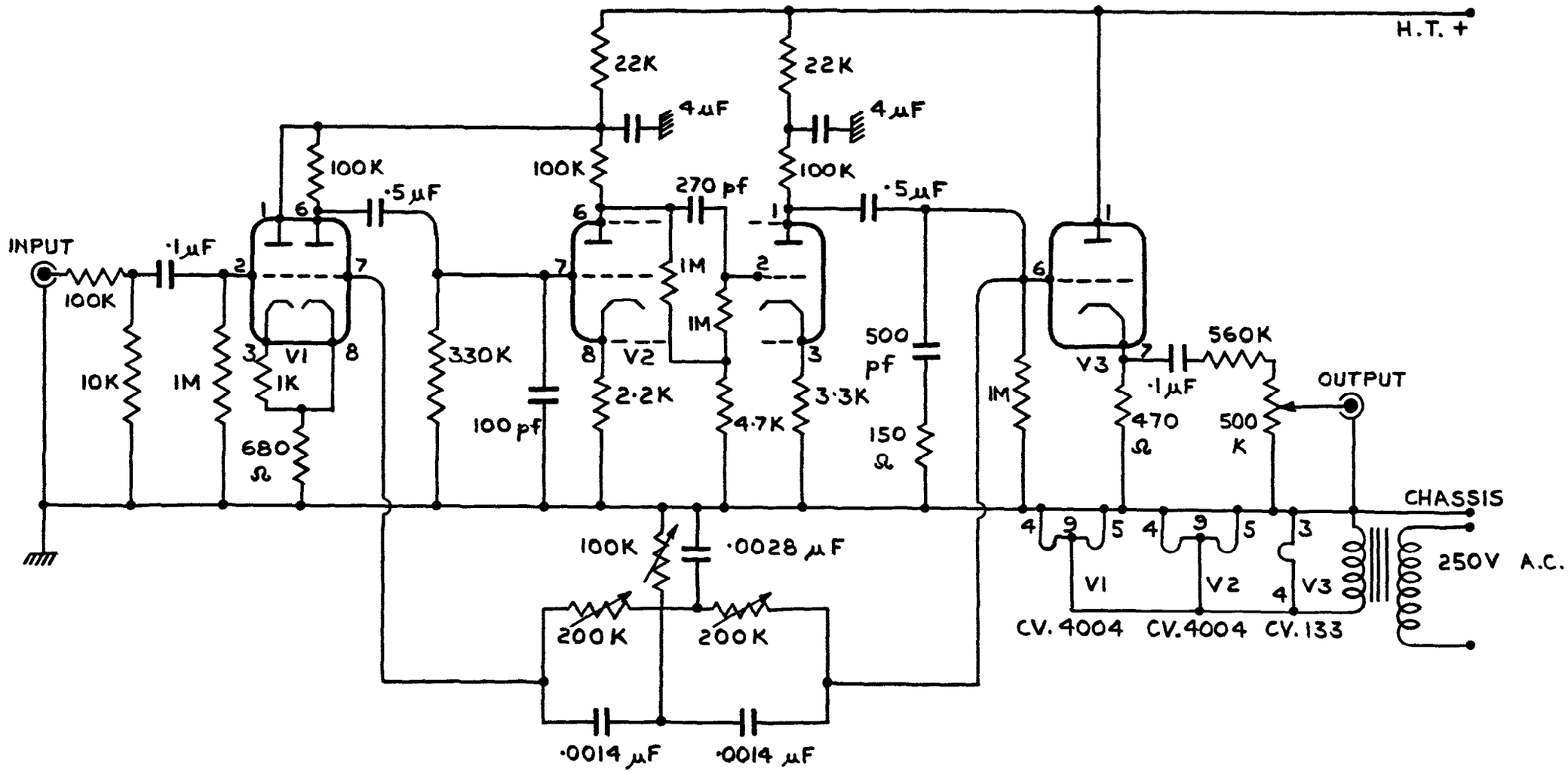

FIG. 7. VALVE FILTER CIRCUIT FOR USE IN ELLIOTT STRAIN GAUGE EQUIPMENT.

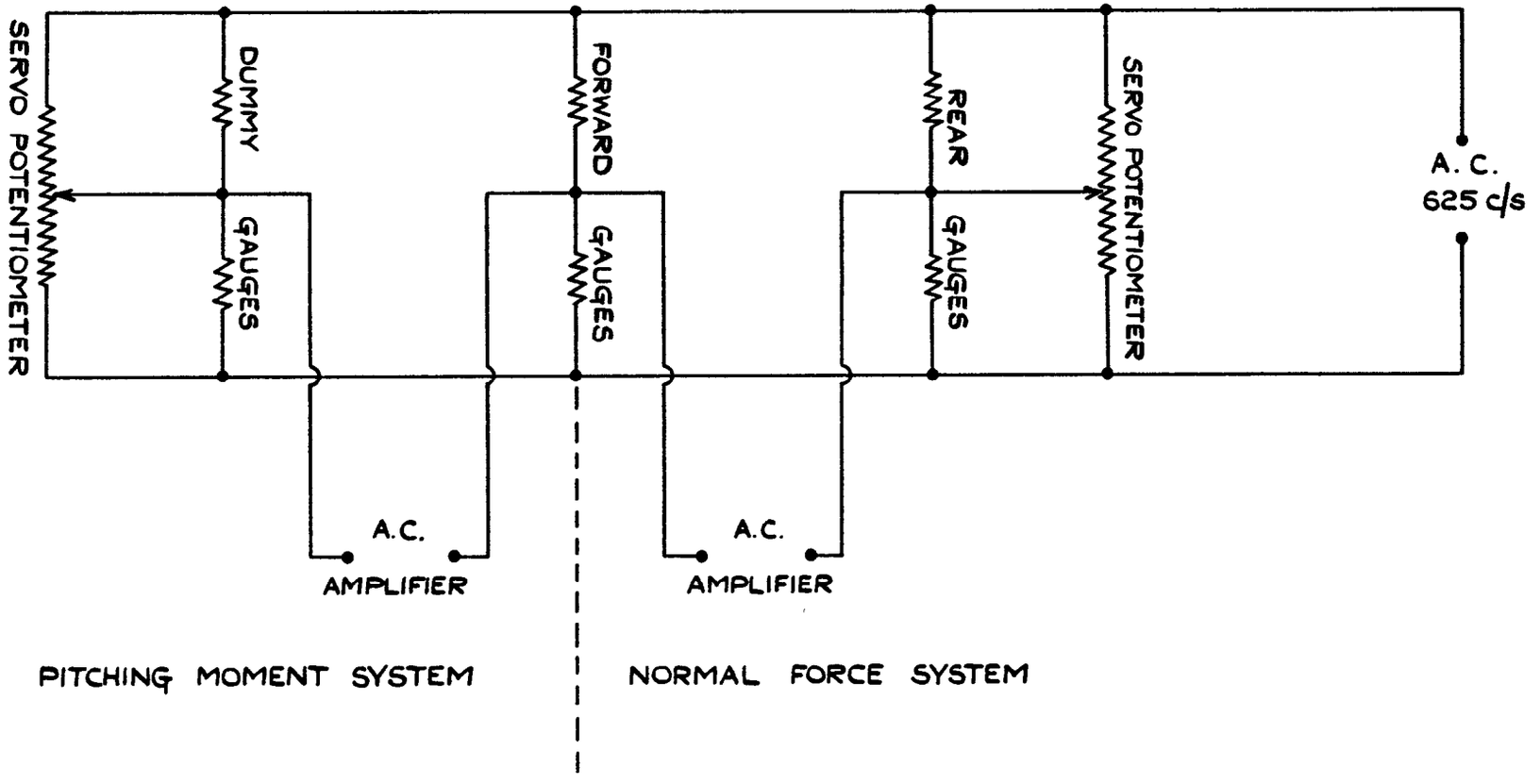

FIG. 8. BACK-TO-BACK SERVO SYSTEM FOR SIMULTANEOUS READING OF NORMAL FORCE AND PITCHING MOMENT FROM TWO GAUGE STATIONS.

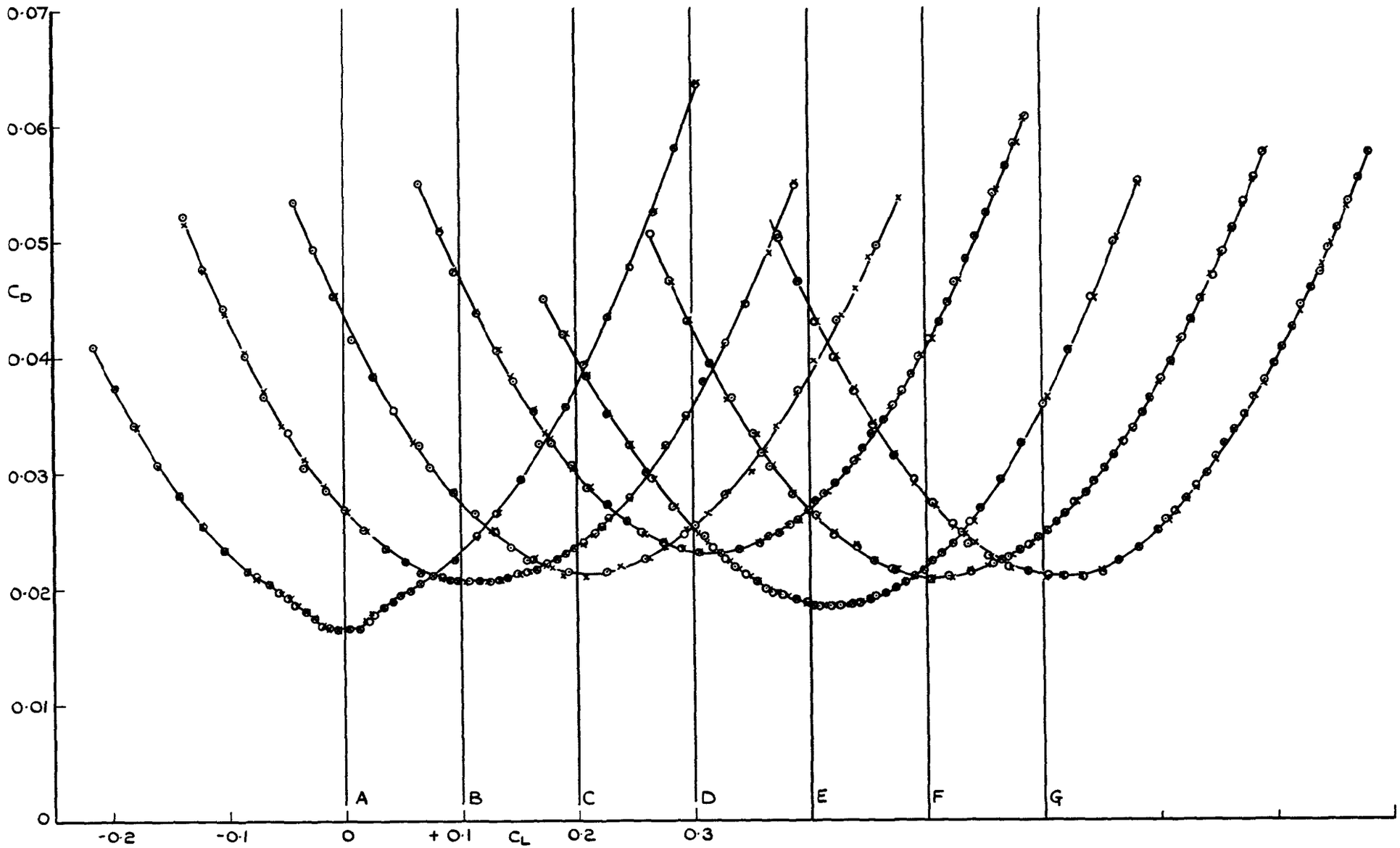

FIG.9. DRAG POLARS — TRANSITION FREE
MACH NUMBER 1·4
COEFFICIENTS BASED ON DEVELOPED AREA

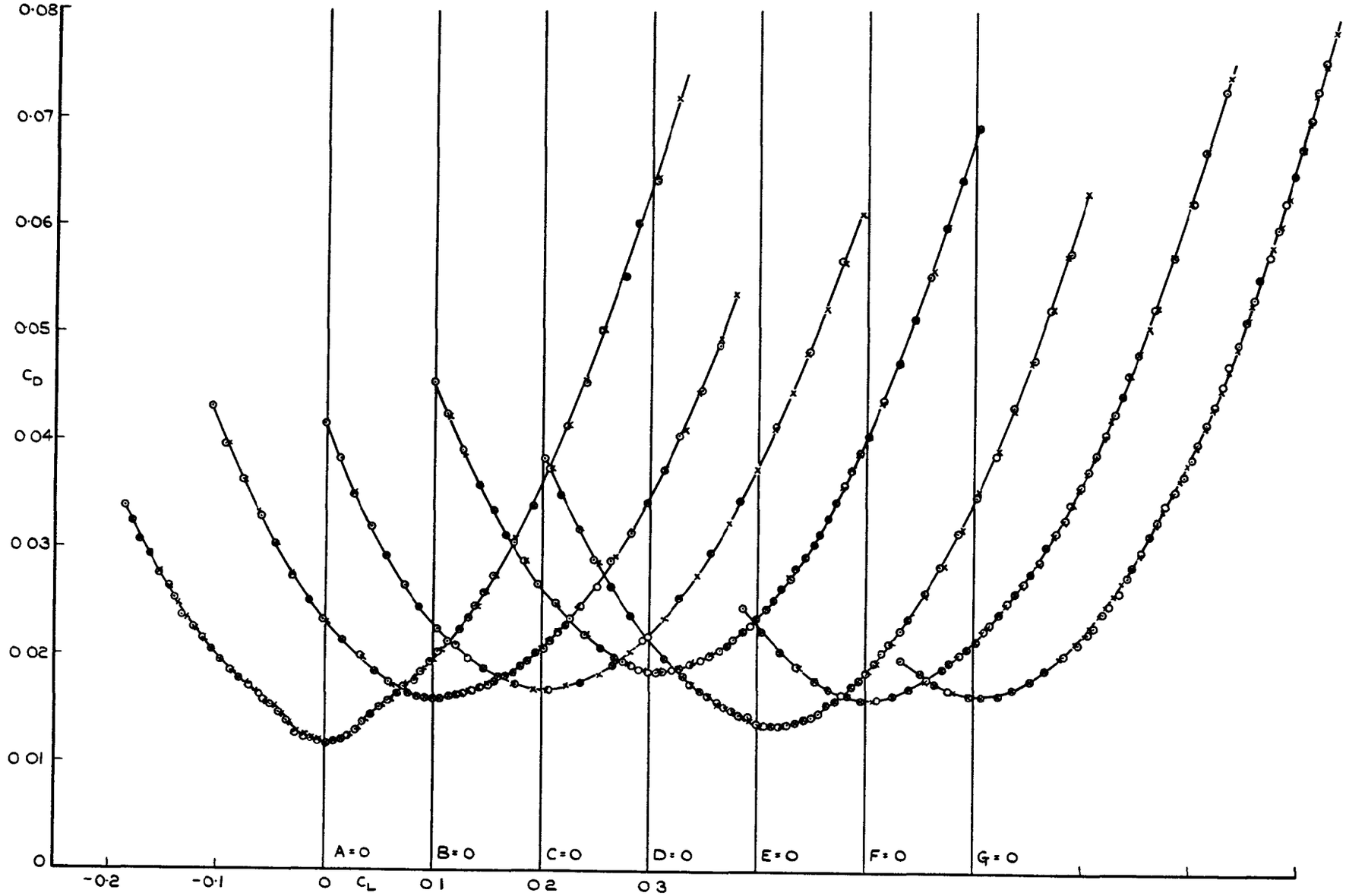

FIG. 10. DRAG POLARS - TRANSITION FREE
MACH NUMBER 1·8
COEFFICIENTS BASED ON DEVELOPED AREA

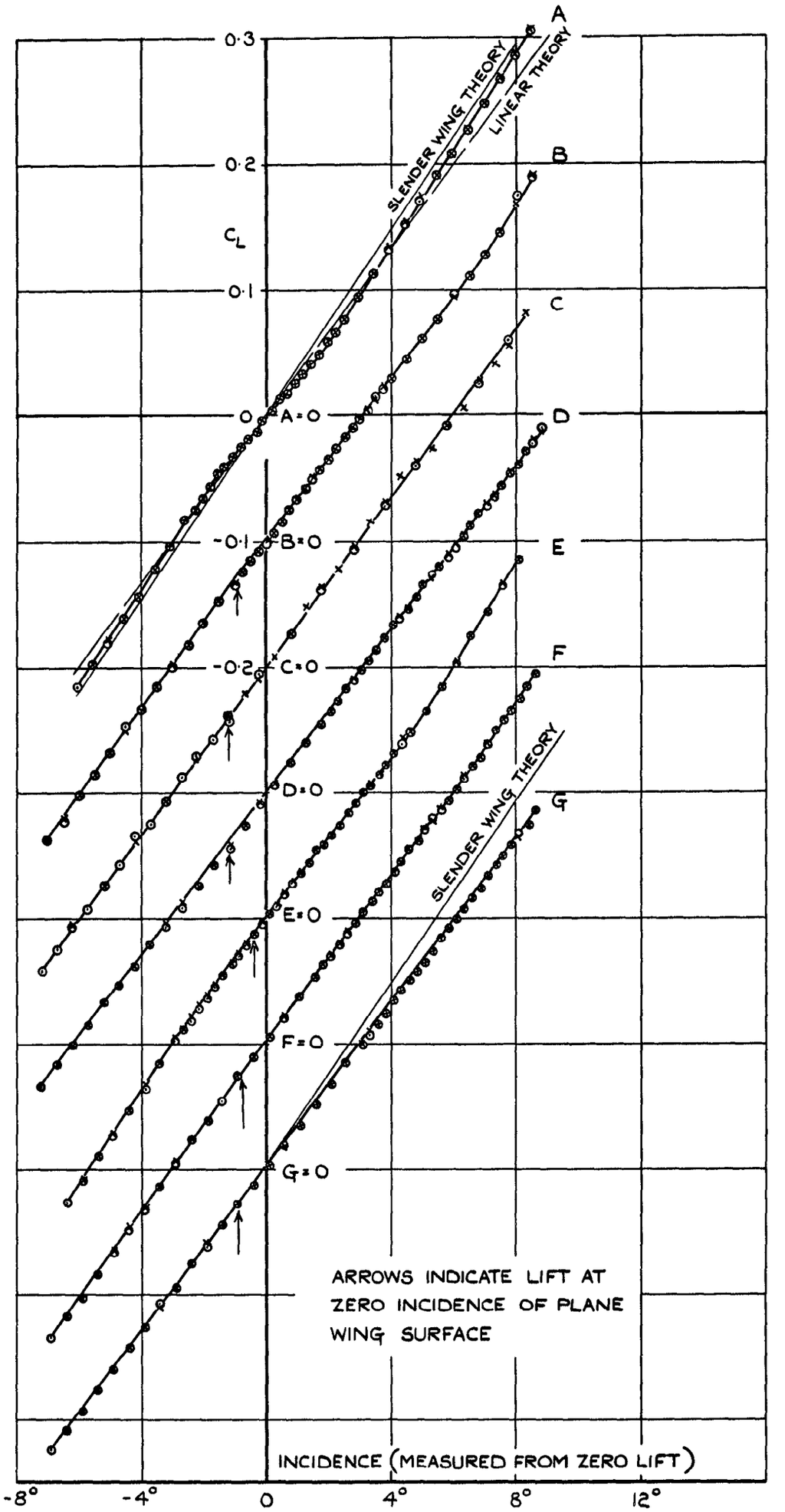

FIG.11. LIFT CURVES OF ALL WINGS AT M=1·4.
(COEFFICIENT BASED ON DEVELOPED AREA)

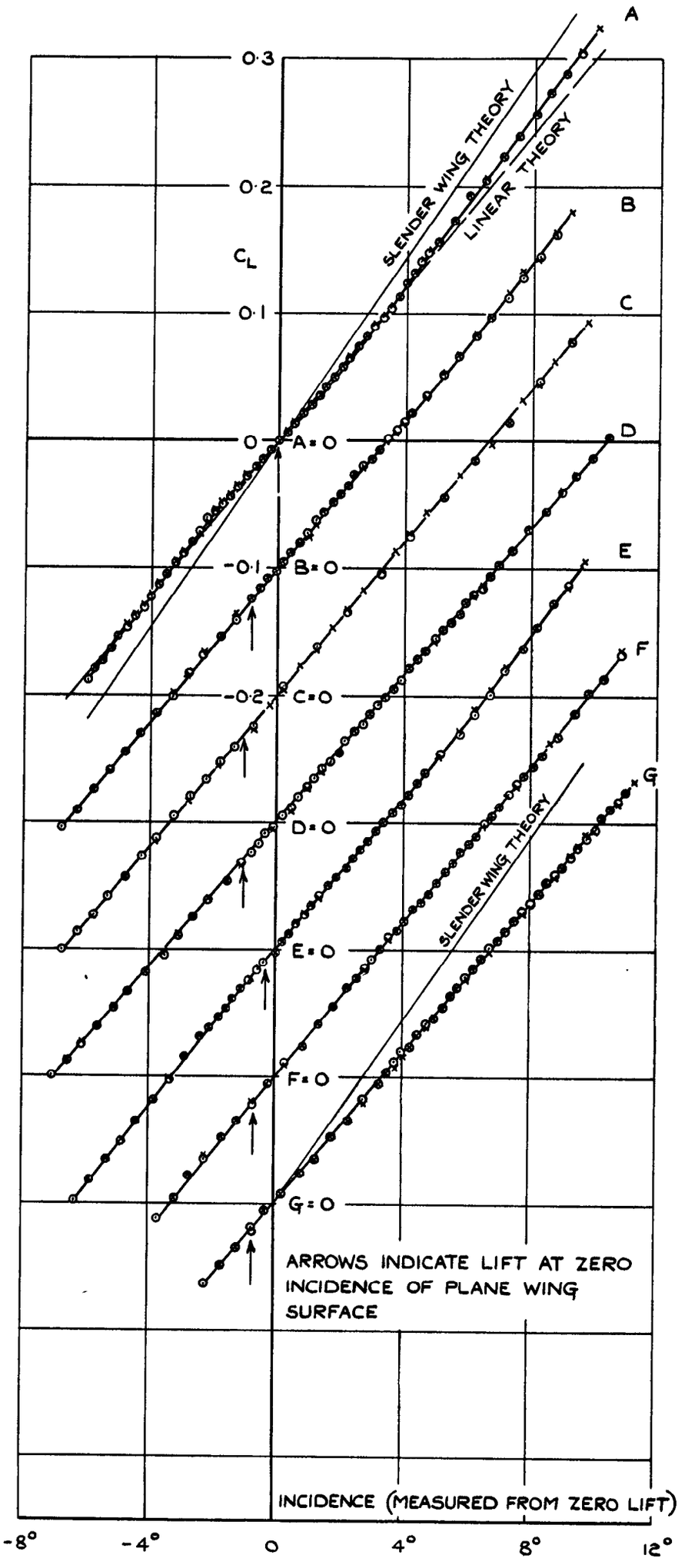

FIG.12. LIFT CURVES OF ALL WINGS AT M=1·8.
(COEFFICIENT BASED ON DEVELOPED AREA)

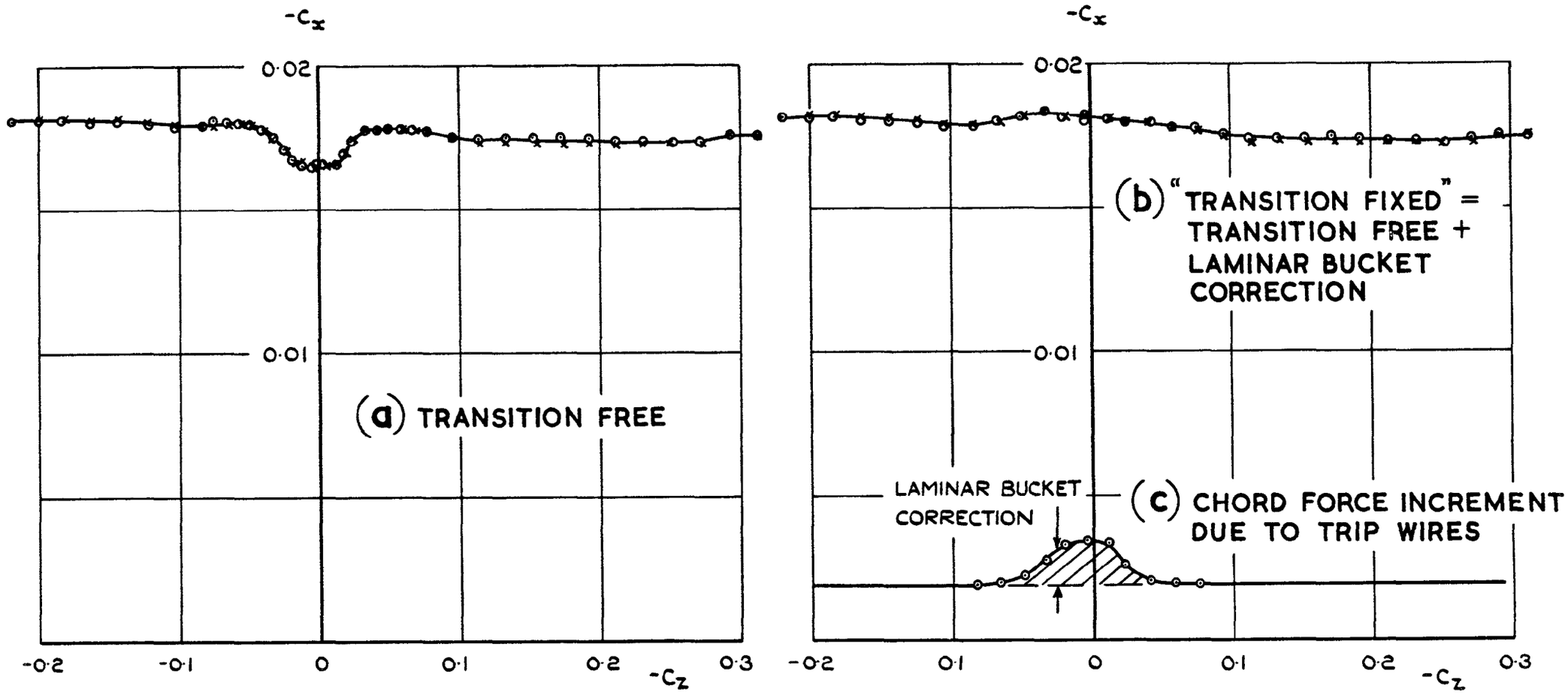

FIG. 13. CHORD FORCE v NORMAL FORCE (ZERO LIFT AXES)
WING A. MACH NUMBER 1·4.

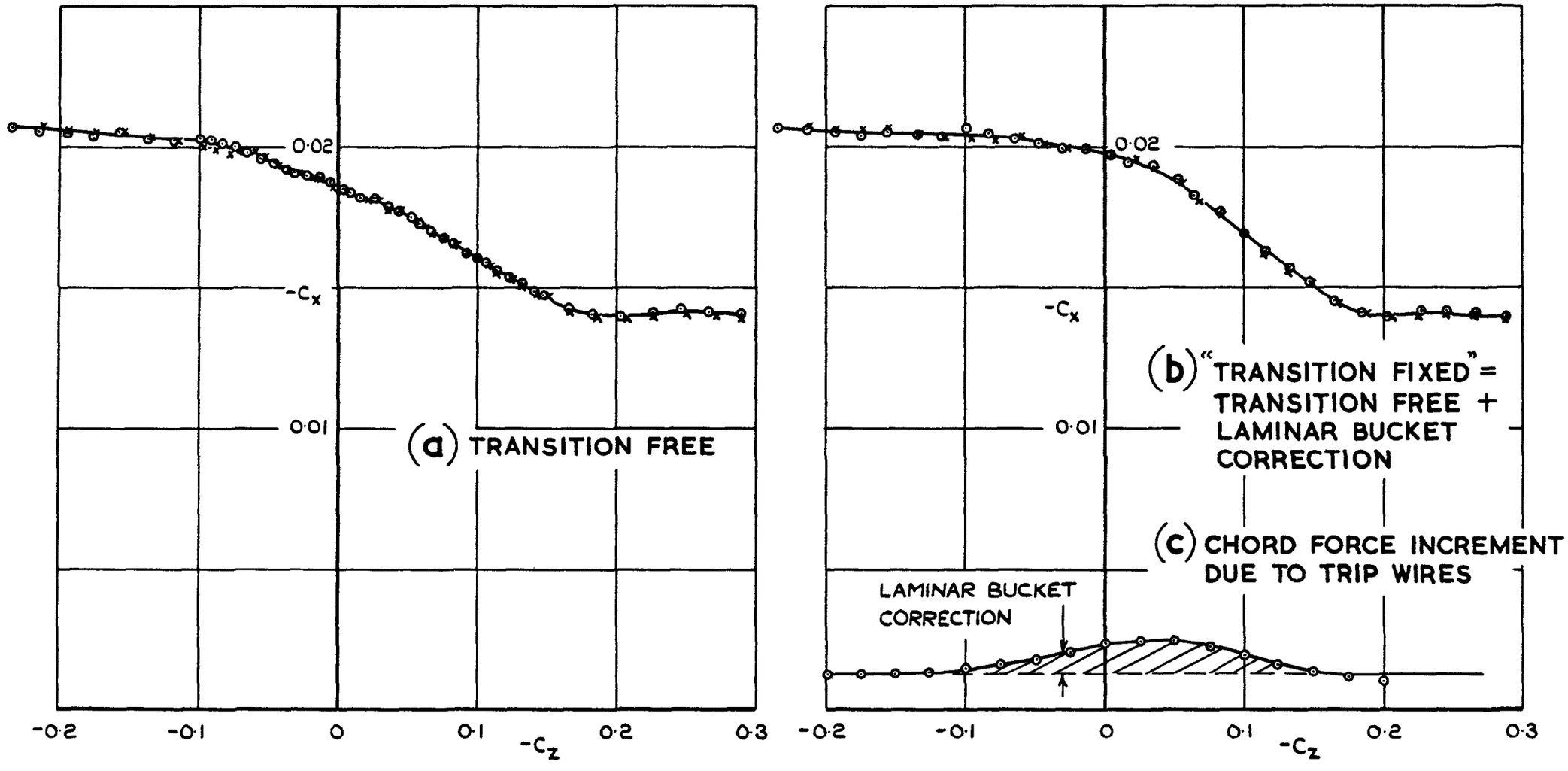

FIG.14. CHORD FORCE v NORMAL FORCE (ZERO LIFT AXES)
WING E. MACH NUMBER 1·4.

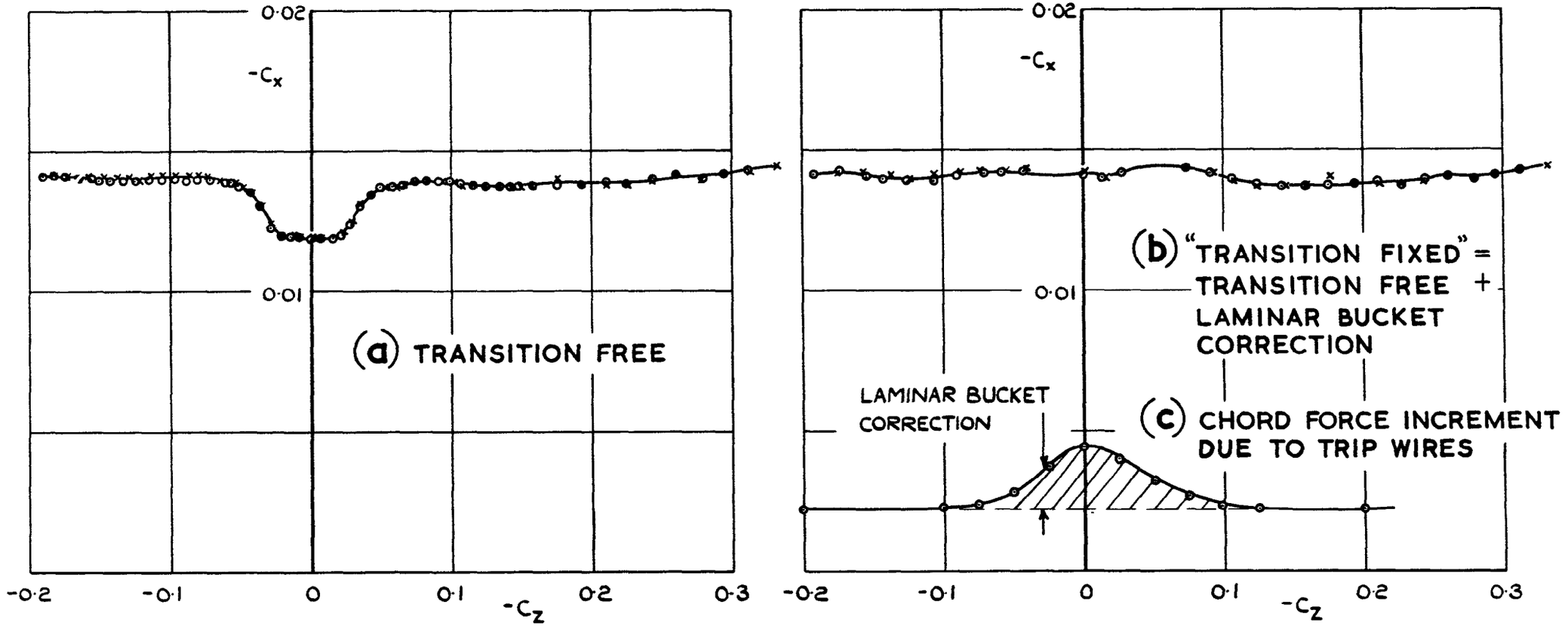

FIG.15. CHORD FORCE v NORMAL FORCE (ZERO LIFT AXES)
WING A. MACH NUMBER 1·8.

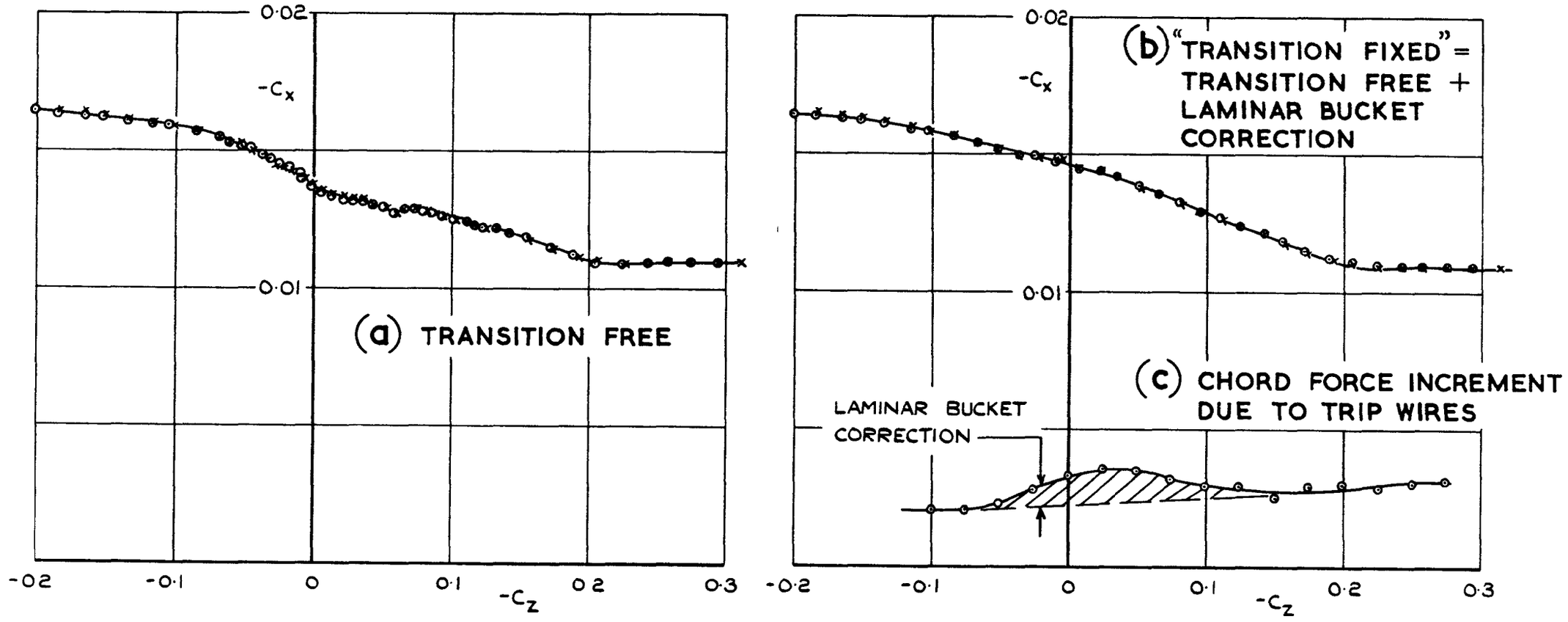

FIG.16. CHORD FORCE v NORMAL FORCE (ZERO LIFT AXES)
WING E. MACH NUMBER 1·8.

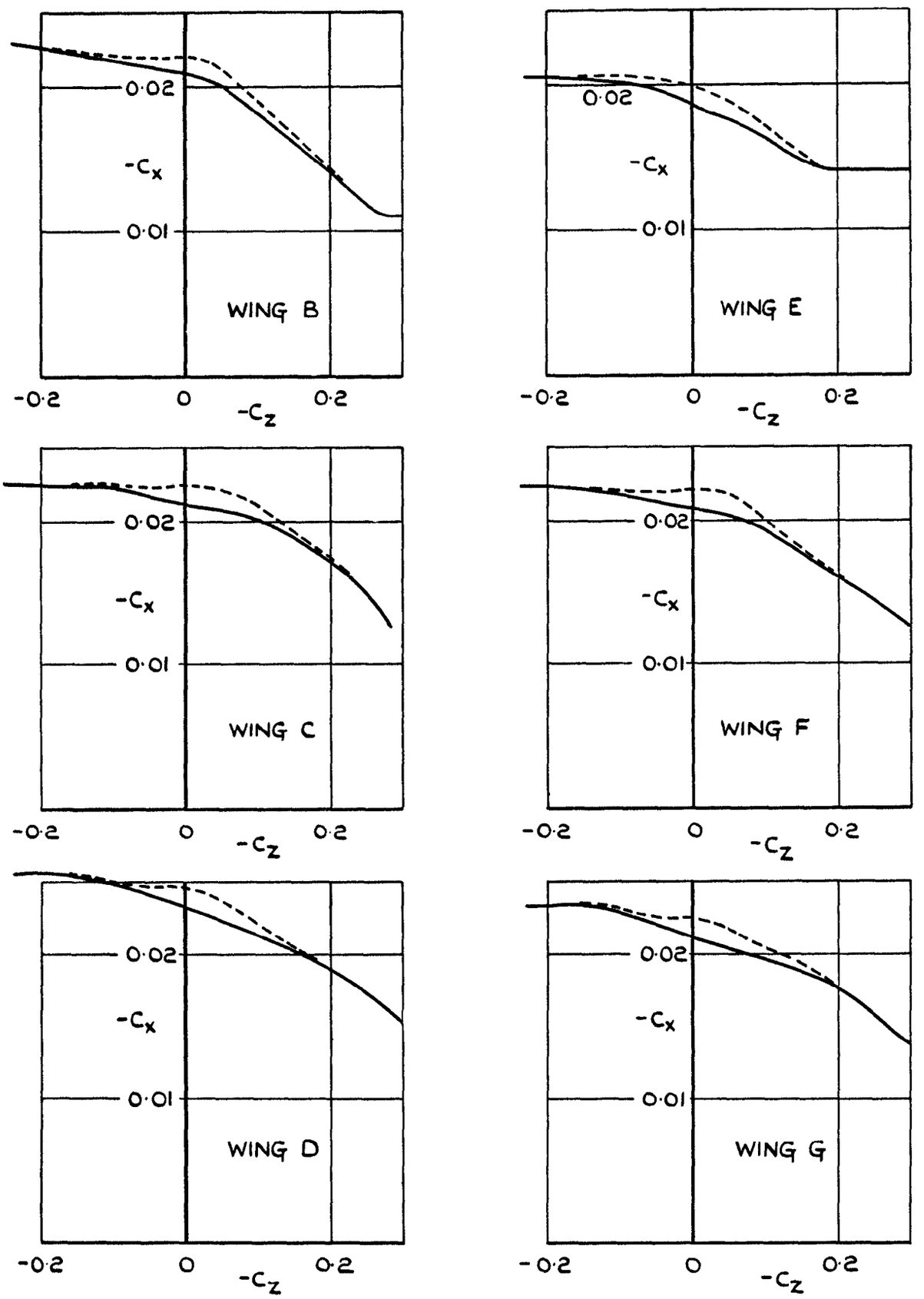

TRANSITION FREE ——

WING E LAMINAR BUCKET CORRECTION - - - - -

FIG. 17. CHORD FORCE v NORMAL FORCE (ZERO LIFT AXES) ALL CAMBERED WINGS AT M=1·4 TRANSITION FREE AND "TRANSITION FIXED".

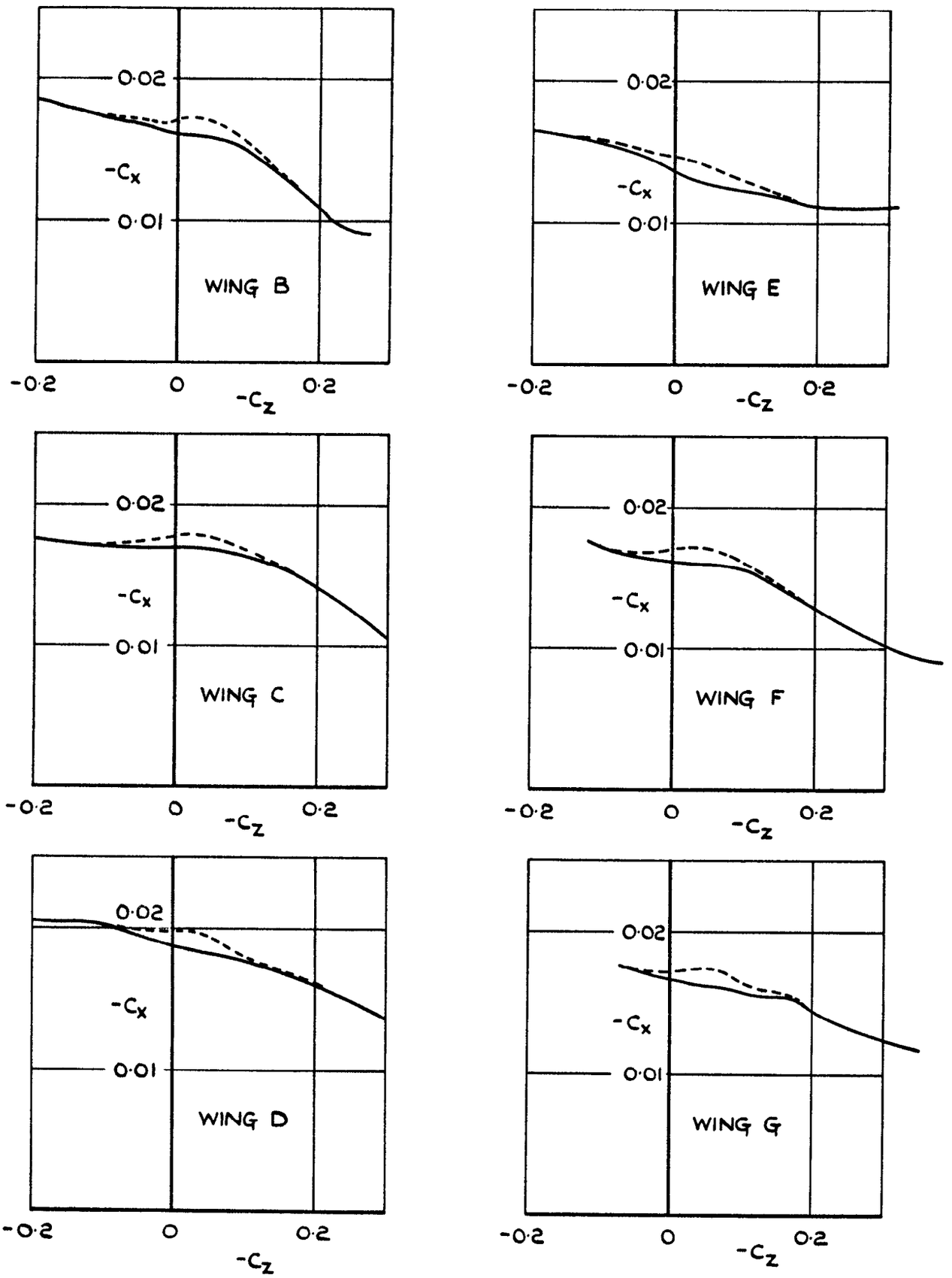

FIG.18. CHORD FORCE v NORMAL FORCE (ZERO LIFT AXES) ALL CAMBERED WINGS AT M=1·8 TRANSITION FREE AND "TRANSITION FIXED."

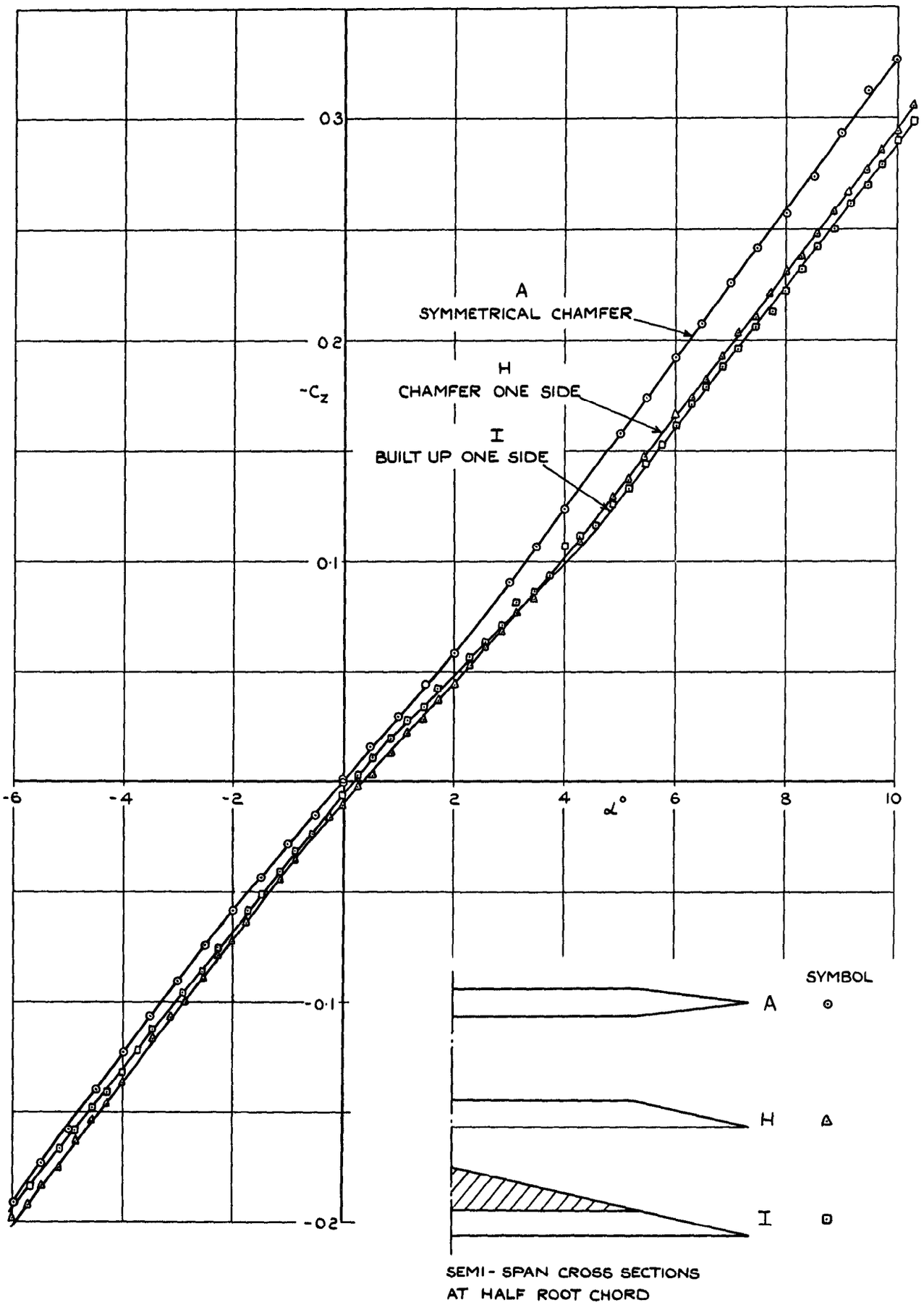

FIG.19. EFFECT ON LIFT OF DIFFERENT CHAMFERS ON UNCAMBERED DELTA WING AT M=1·8.

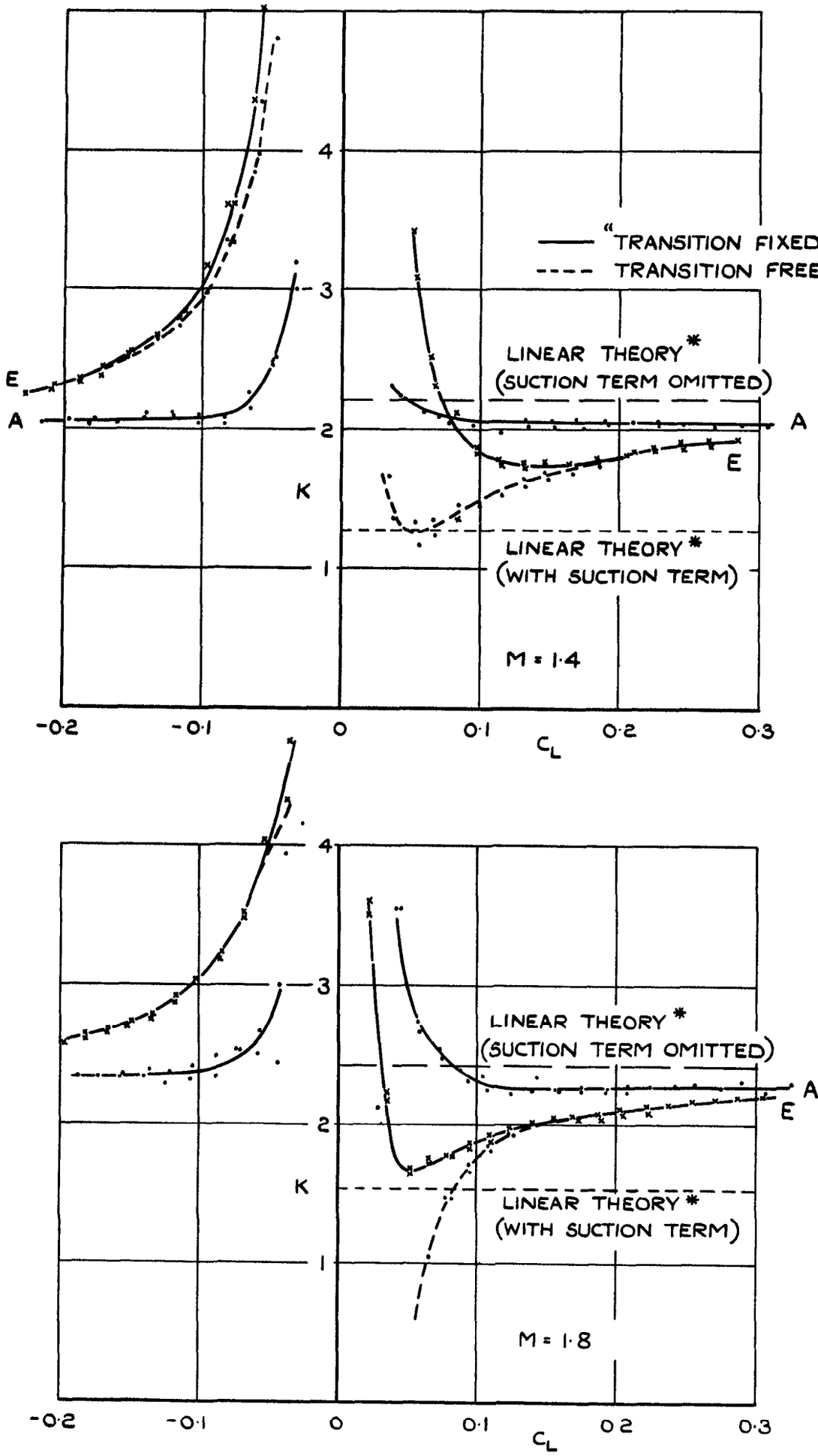

* LINEAR THEORY FOR FLAT DELTA WING WITH SUBSONIC LEADING EDGES

FIG. 20. LIFT-DEPENDENT DRAG FACTOR OF WINGS A AND E, M = 1·4 AND 1·8.

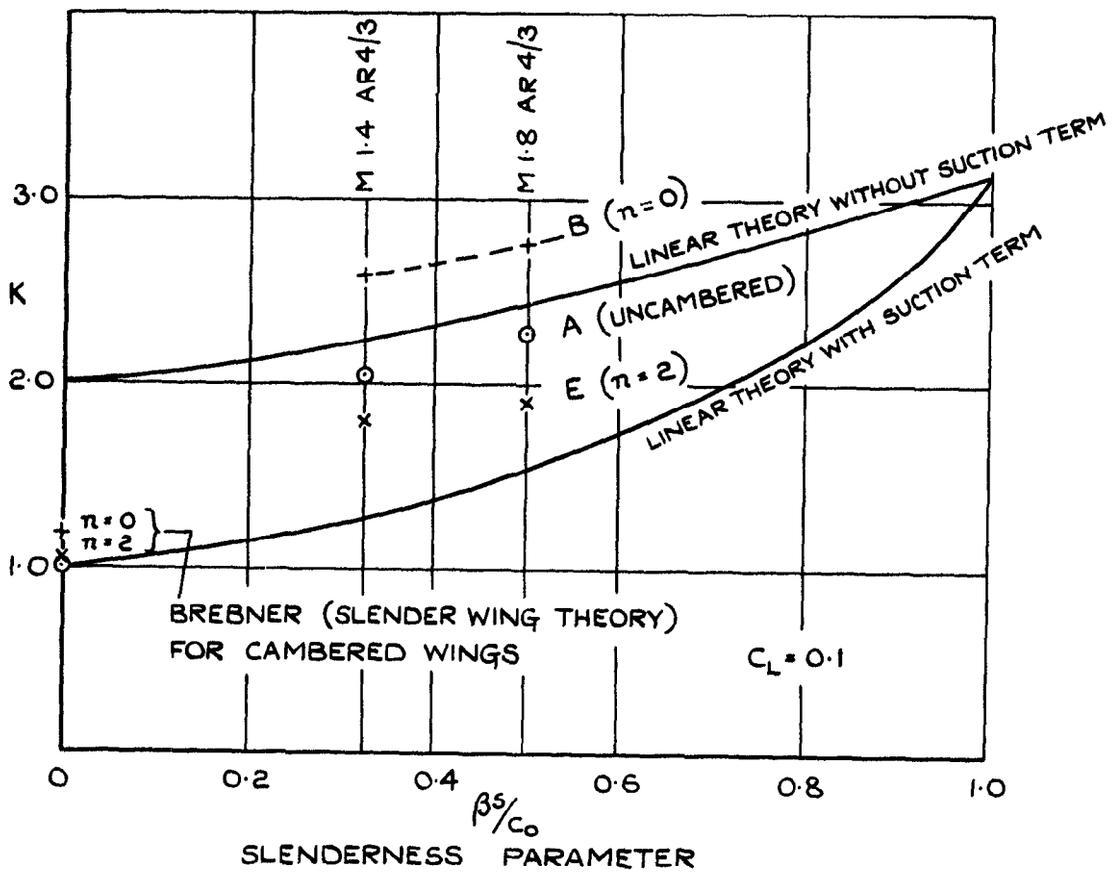

FIG. 21. LIFT-DEPENDENT DRAG FACTOR v SLENDERNESS PARAMETER. UNCAMBERED WING AND WINGS DESIGNED FOR $C_L = 0·1$.

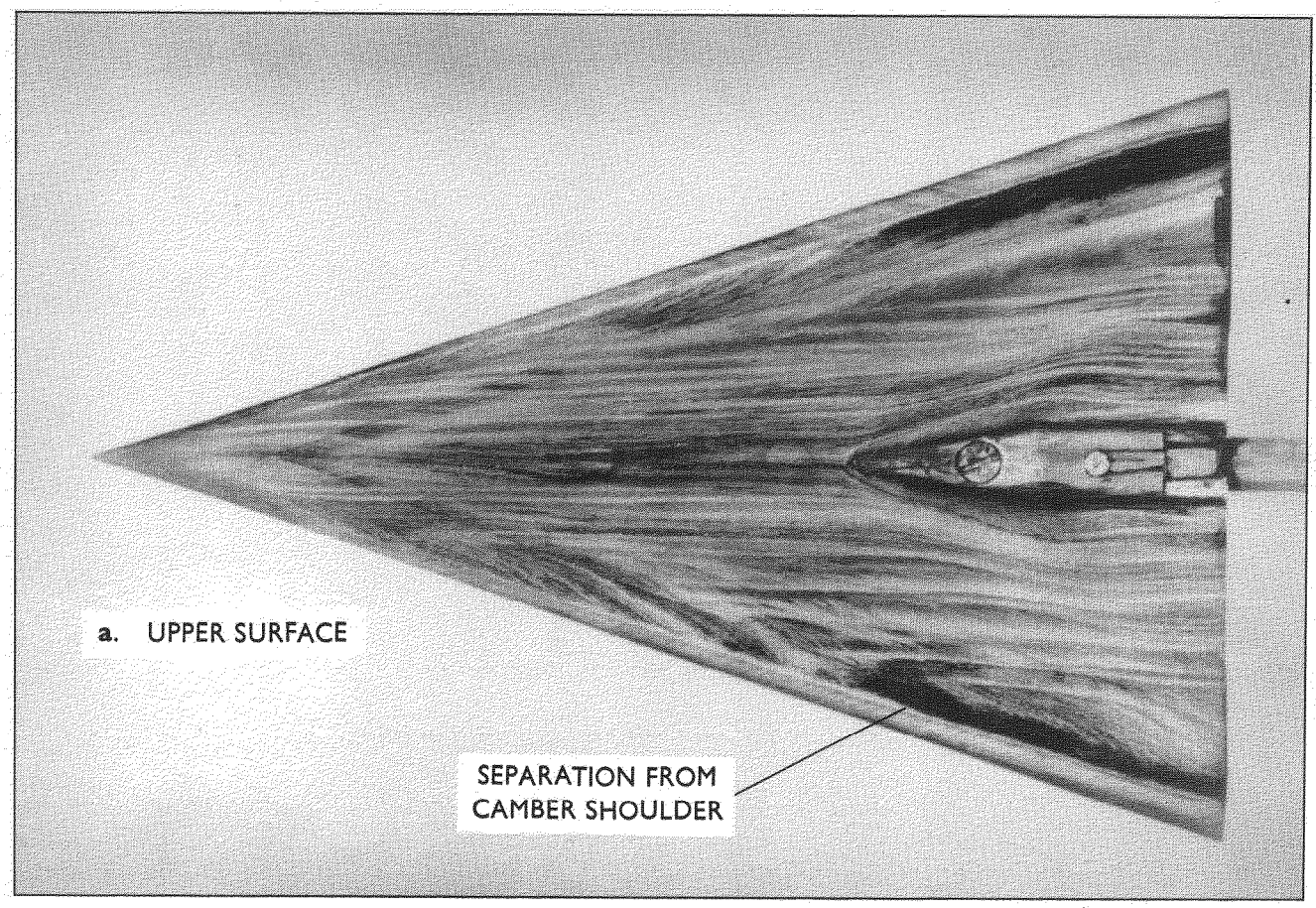

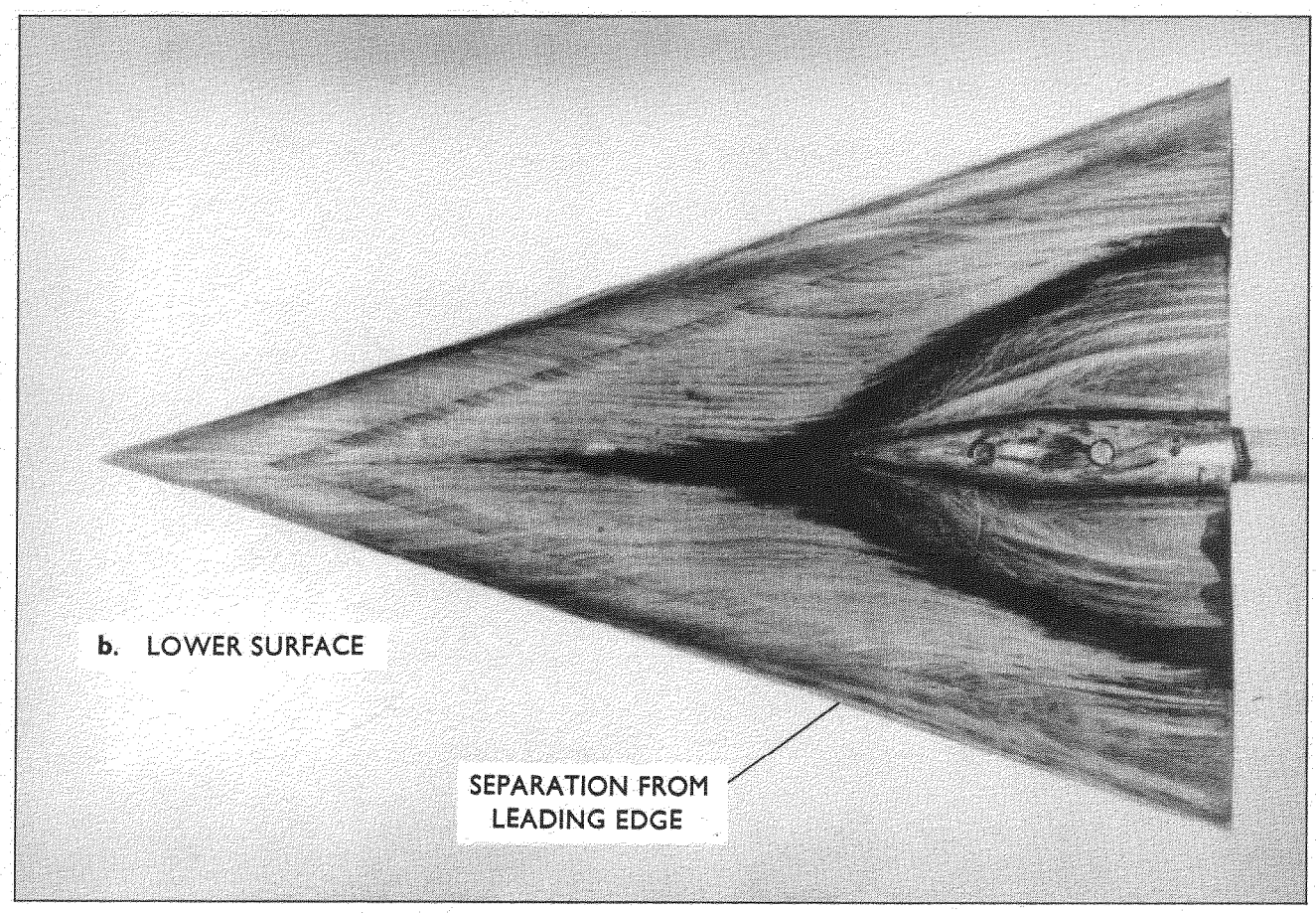

FIG.22. OIL FLOW PATTERN AT DESIGN INCIDENCE.
MODEL 'F', $\alpha = +3\frac{1}{2}°$, MACH No. 1·8

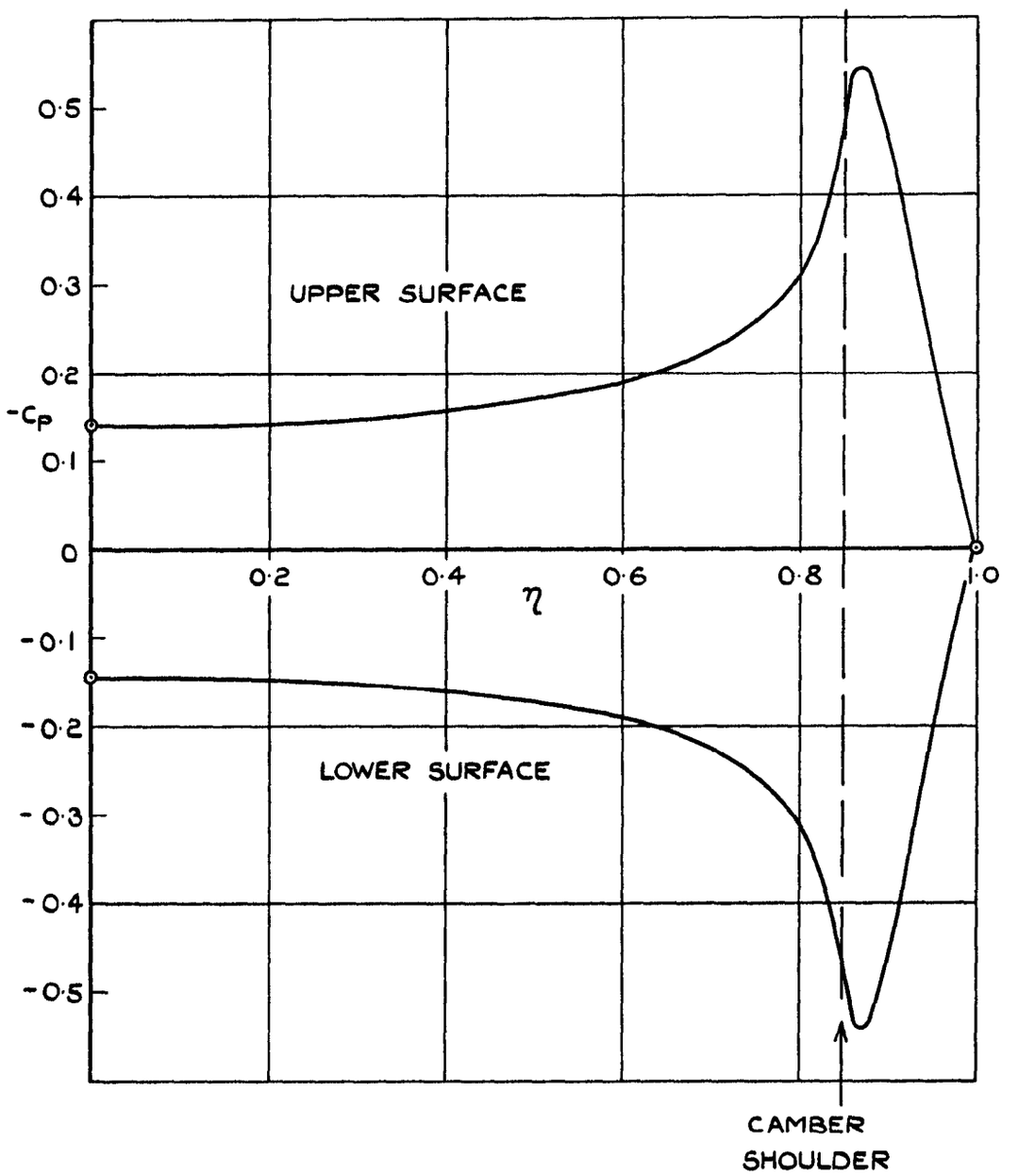

FIG. 23. THEORETICAL SPANWISE PRESSURE DISTRIBUTION ON THIN CONICALLY CAMBERED DELTA WING. WING E AT DESIGN C_L

BREBNER $n = 2$

$C_{L_d} = 0.1$

AR $= \frac{4}{3}$

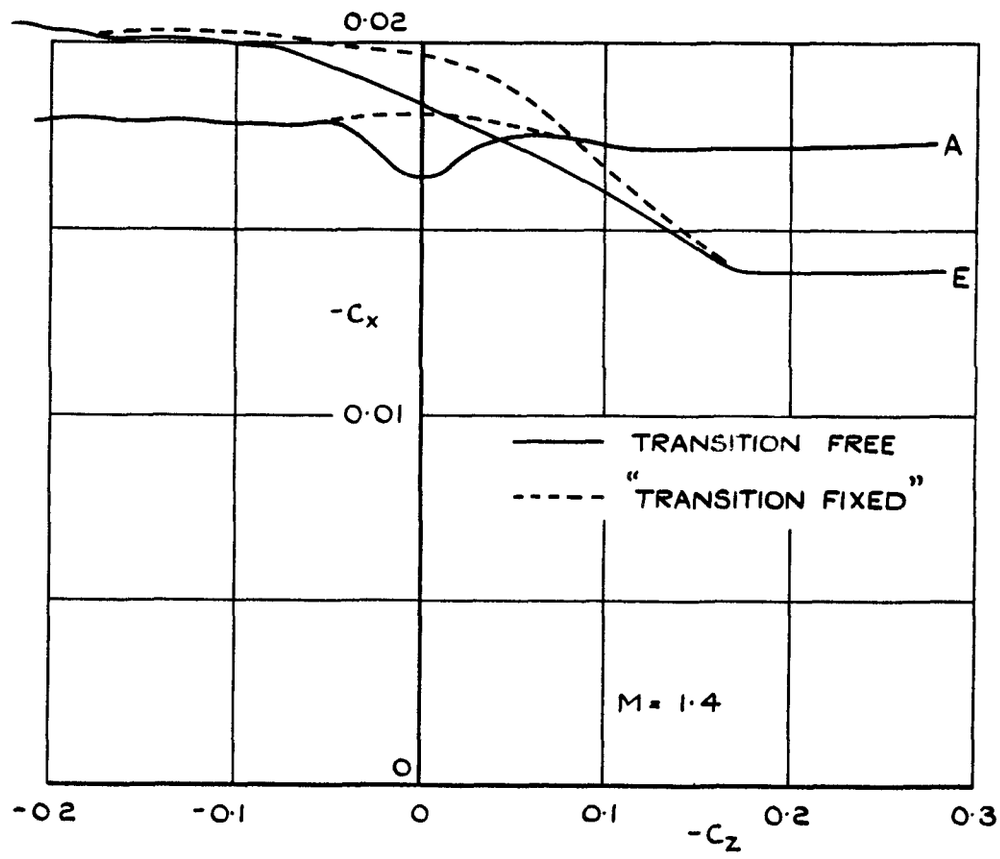

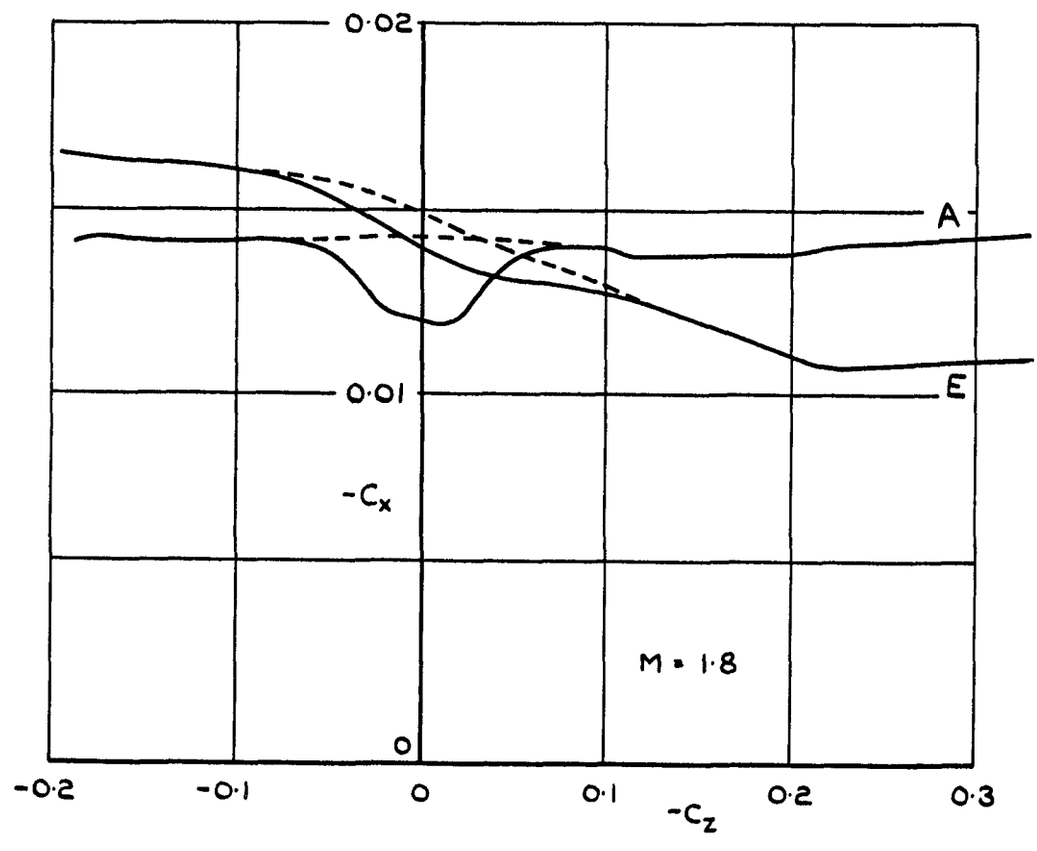

FIG. 24. CHORD FORCE v NORMAL FORCE OF WINGS A AND E COMPARED.

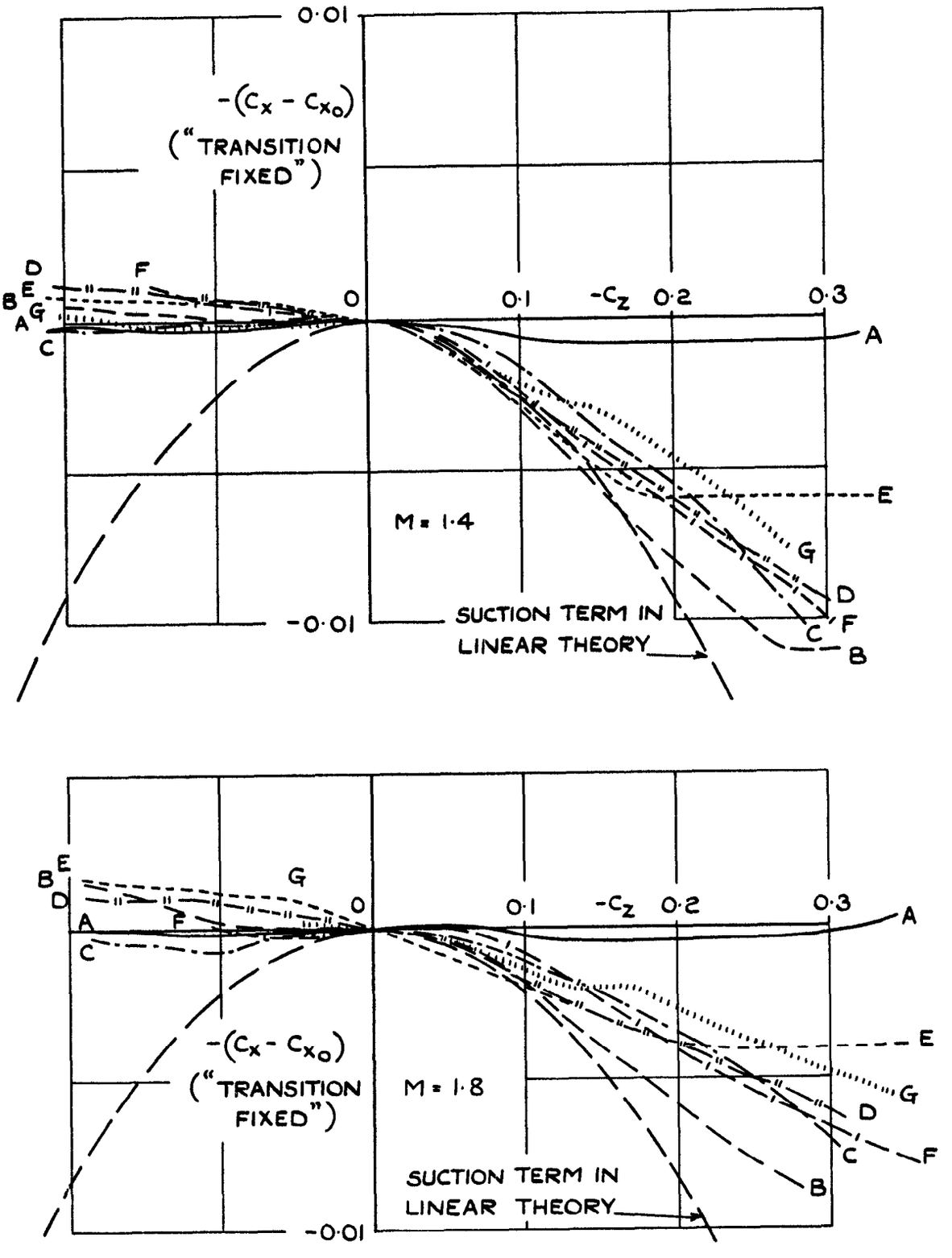

FIG. 25. VARIATION IN CHORD FORCE WITH NORMAL FORCE COMPARED WITH THE SUCTION TERM IN LINEAR THEORY.

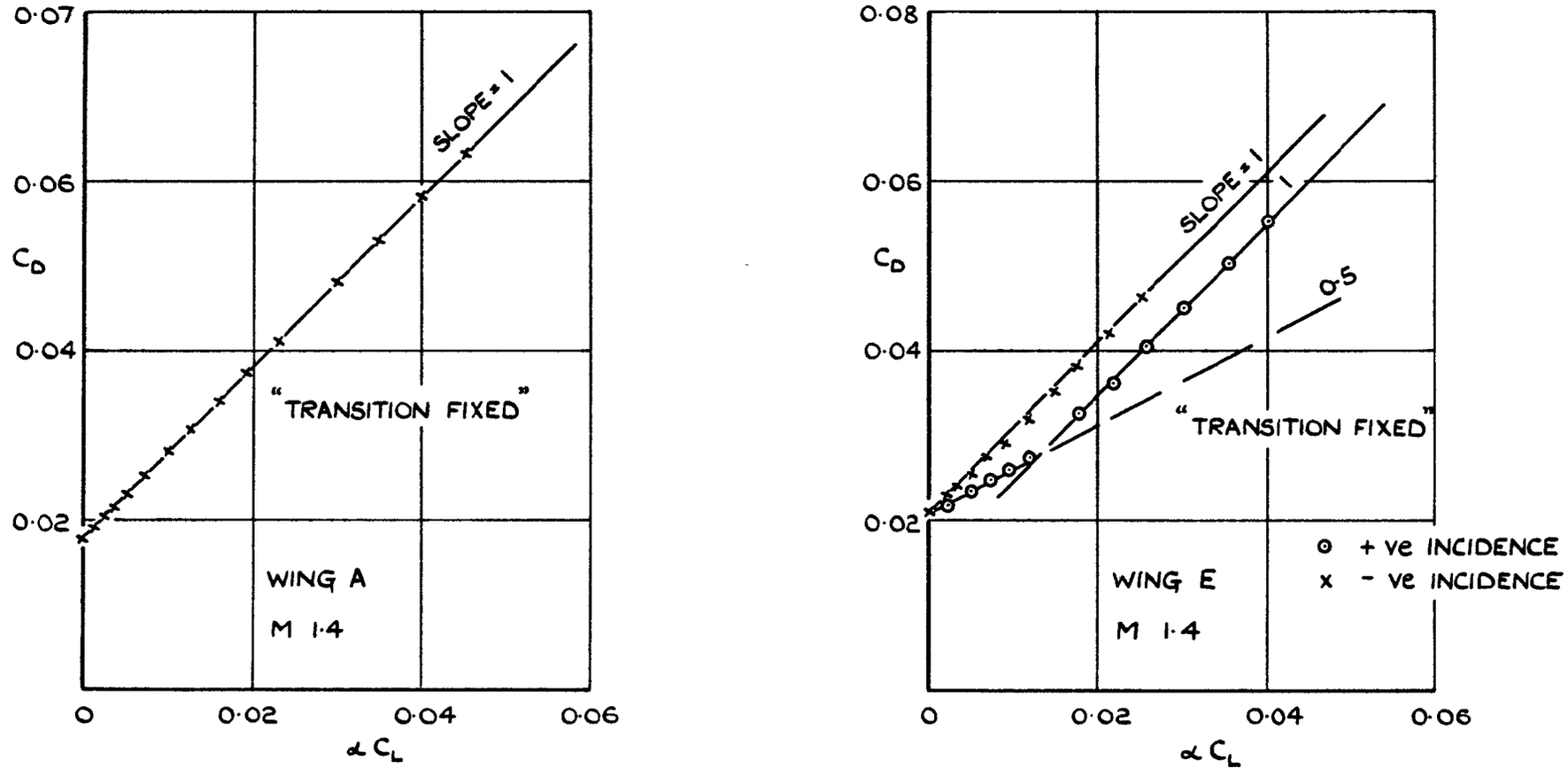

FIG. 26. C_D v αC_L FOR WINGS A AND E
M = 1·4.

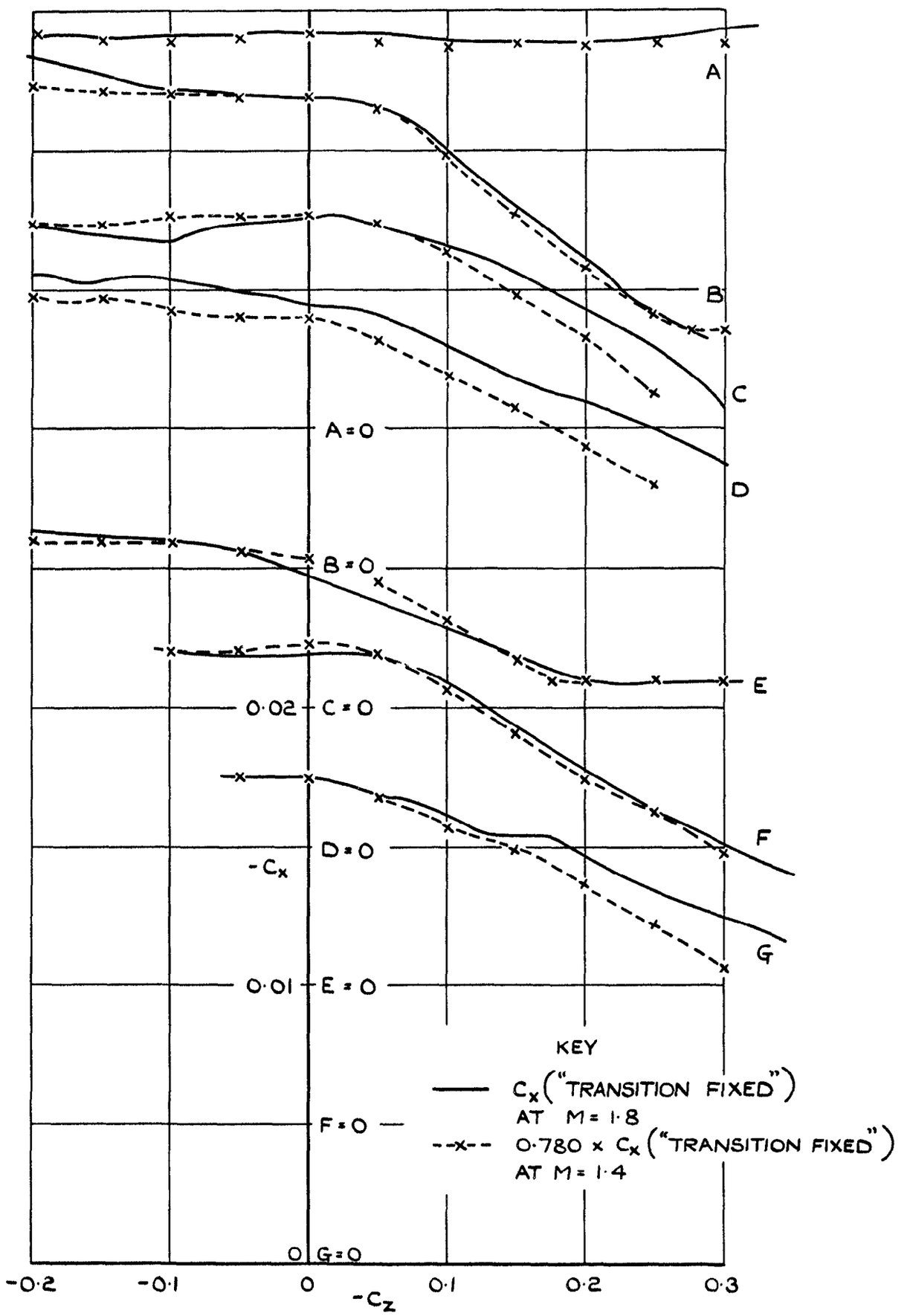

FIG. 27. COMPARISON OF CHORD FORCE RESULTS AT MACH NUMBERS 1·4 AND 1·8.

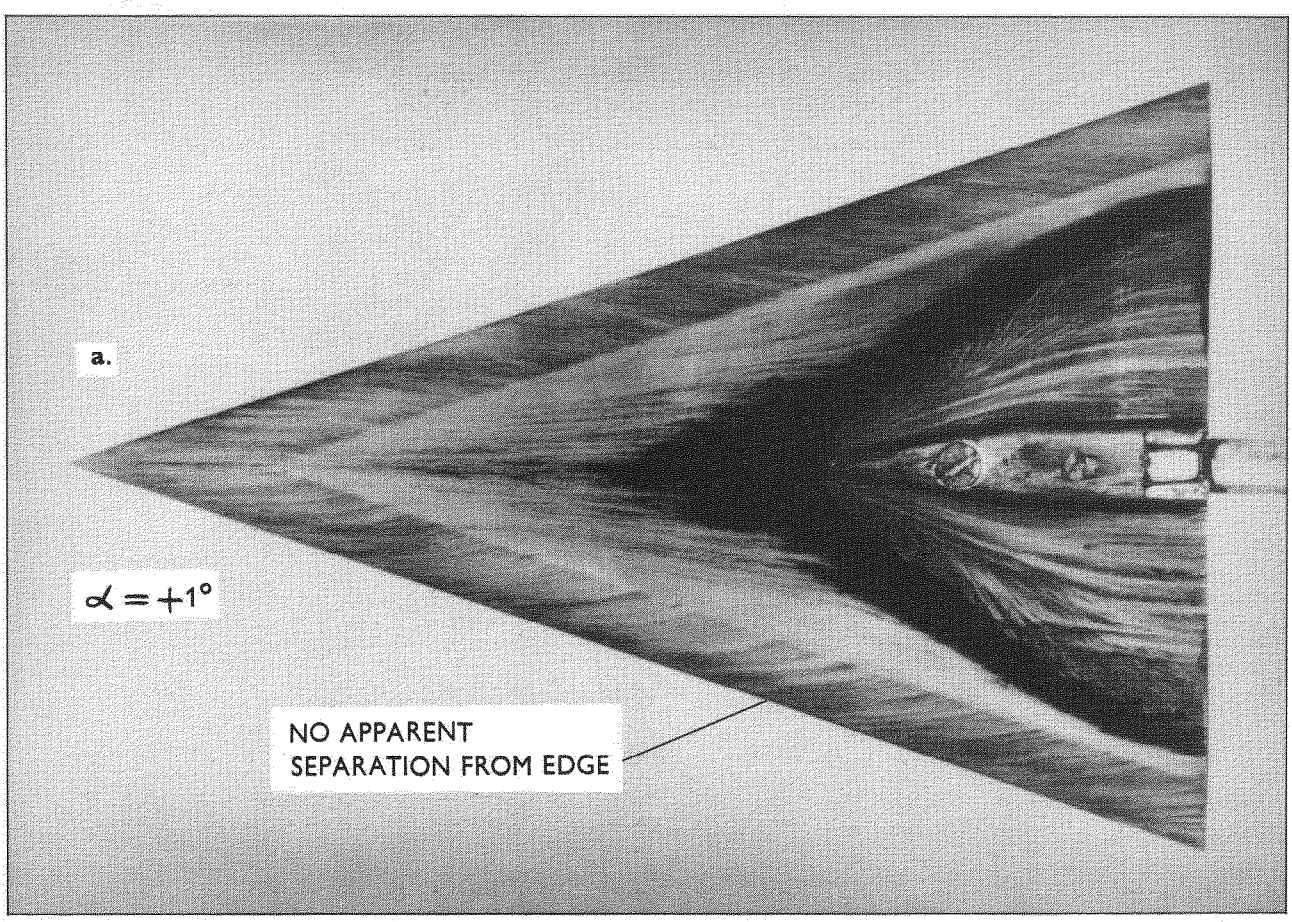

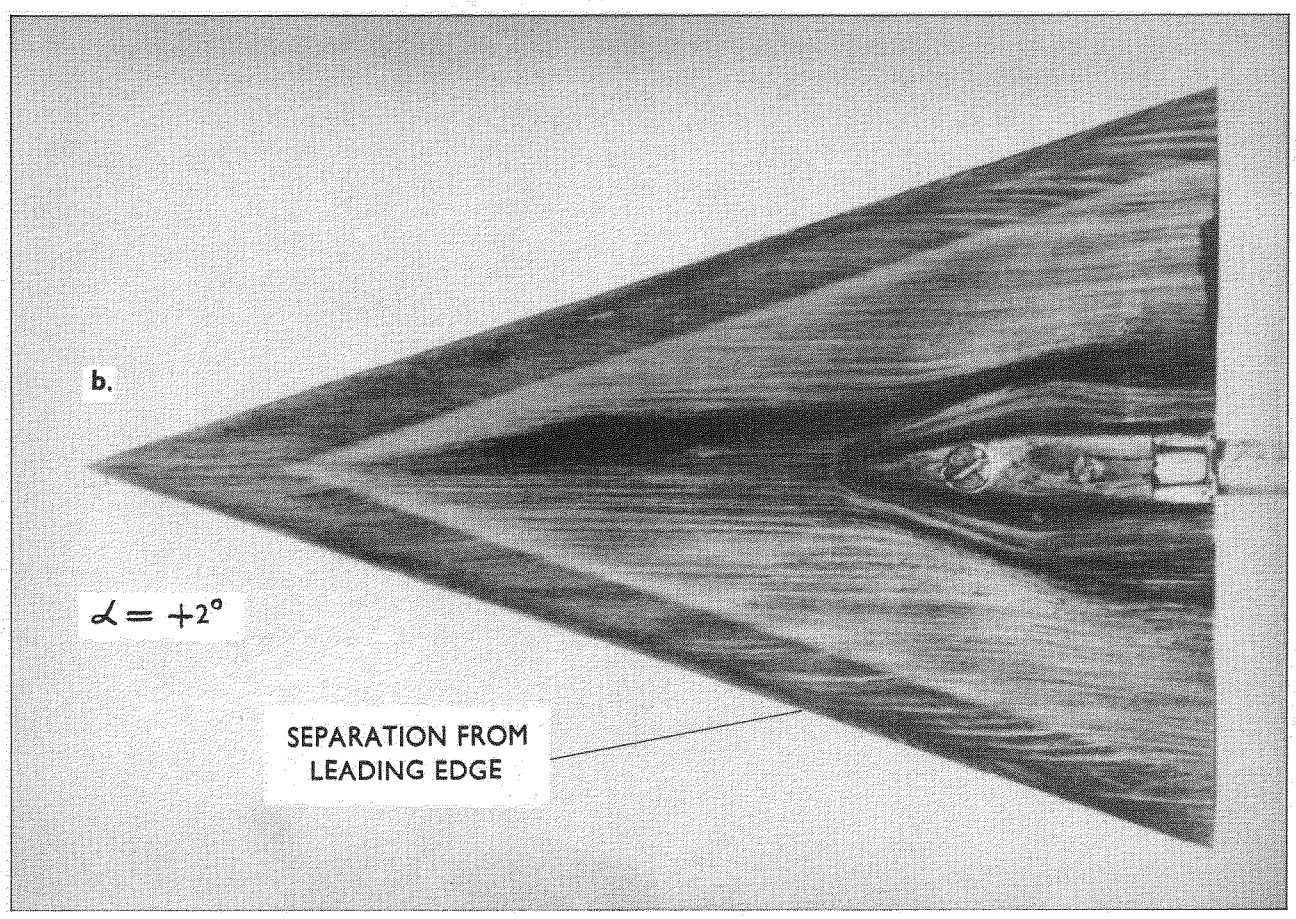

FIG 28 APPEARANCE OF SEPARATION FROM LEADING EDGE OF

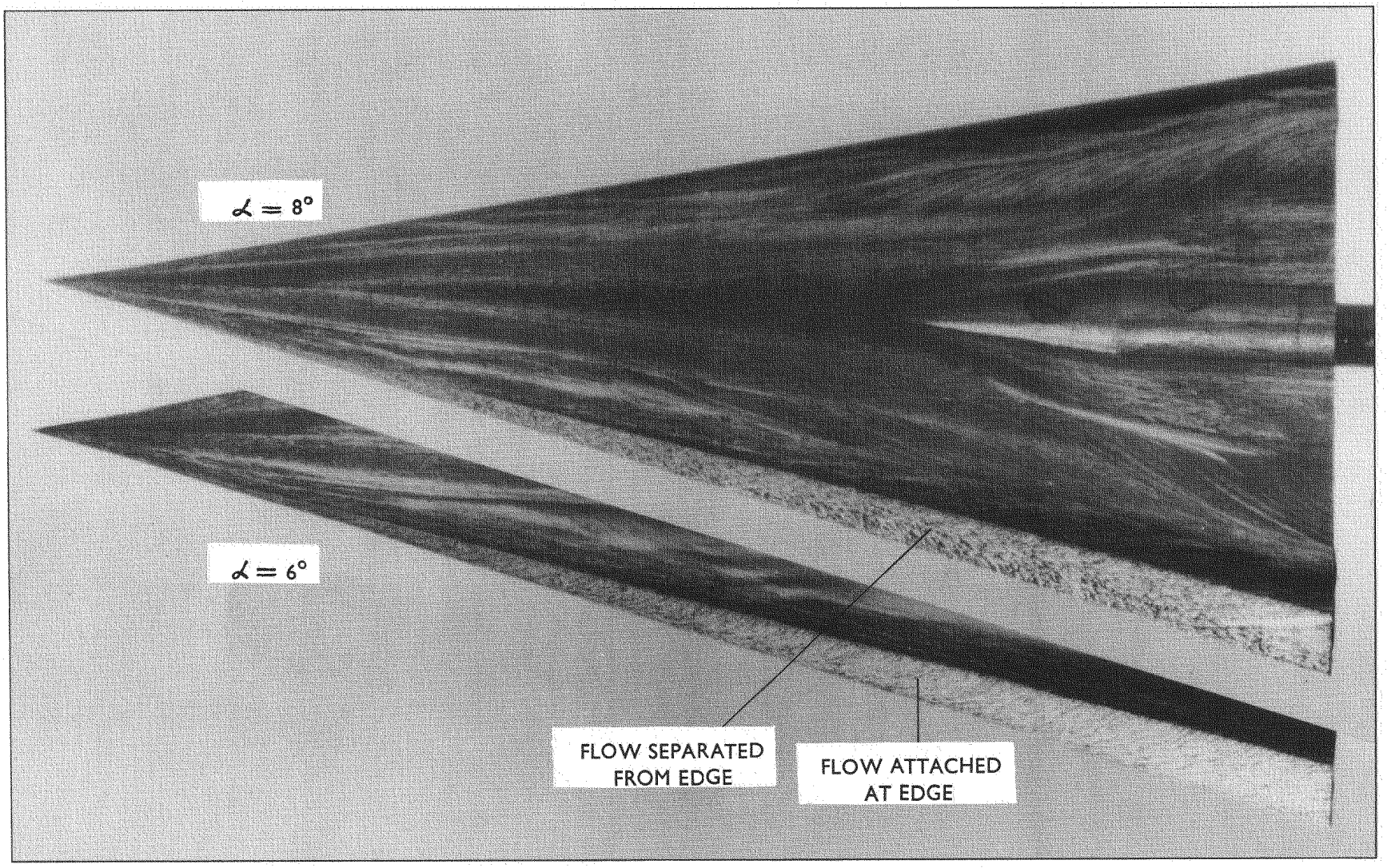

FIG.29. OIL FLOW PATTERN ON OUTER EDGE OF MODEL 'B' AT MACH No. 1·8

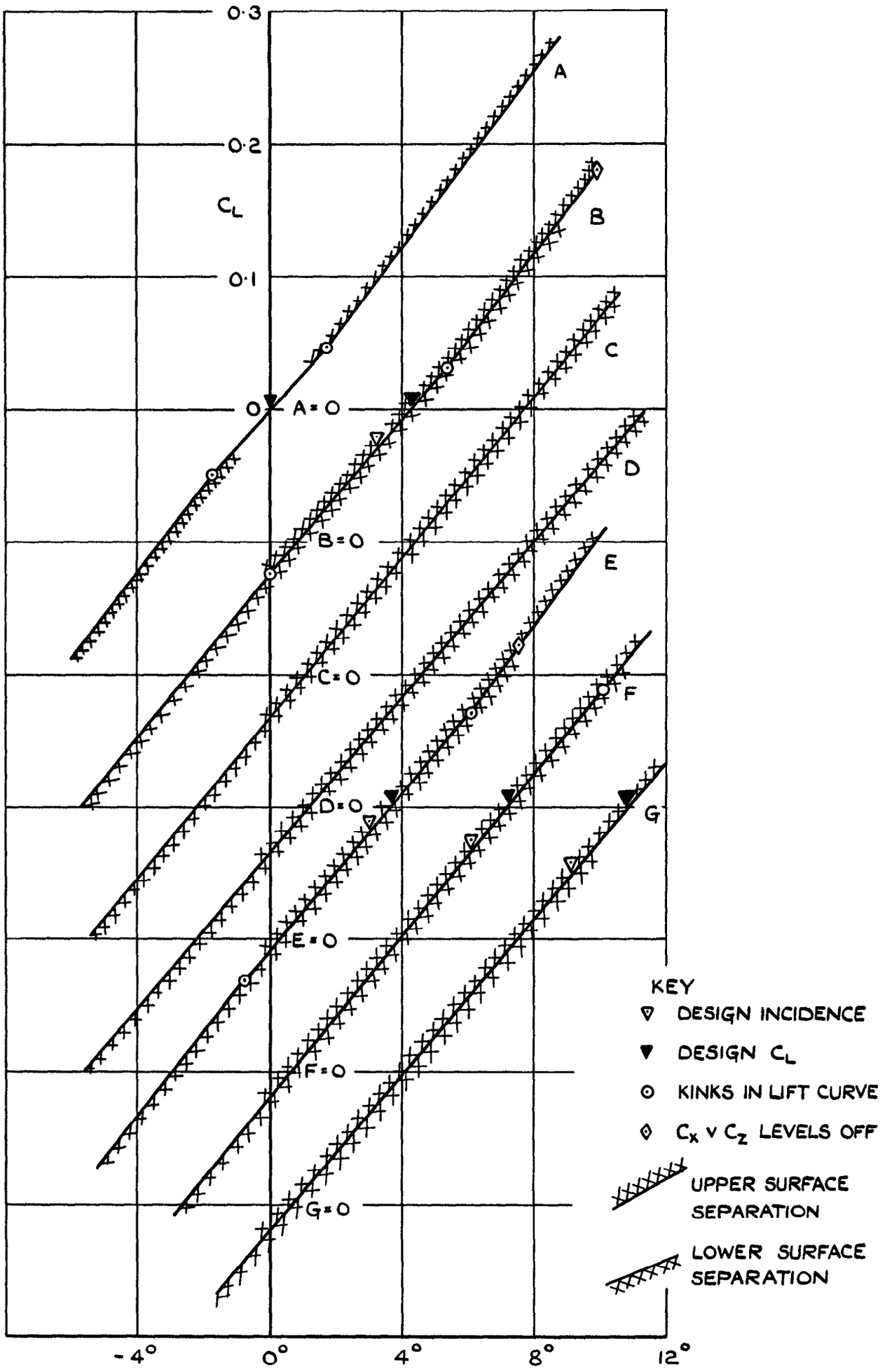

FIG. 30. DIAGRAM SHOWING FORCE AND FLOW CHARACTERISTICS AT M=1·8.

C.P. No. 519
(22,165)
A.R.C. Technical Report

Published by
HER MAJESTY'S STATIONERY OFFICE

To be purchased from
York House, Kingsway, London w.c.2
423 Oxford Street, London w.1
13A Castle Street, Edinburgh 2
109 St. Mary Street, Cardiff
39 King Street, Manchester 2
50 Fairfax Street, Bristol 1
2 Edmund Street, Birmingham 3
80 Chichester Street, Belfast 1
or through any bookseller

Printed in England

S.O. Code No. 23-9012-19

C.P. No. 519